

# VLA-Pruner: Temporal-Aware Dual-Level Visual Token Pruning for Efficient Vision-Language-Action Inference

Ziyan Liu<sup>1,2</sup>, Yeqiu Chen<sup>1,2</sup>, Hongyi Cai<sup>1</sup>, Tao Lin<sup>1</sup>, Shuo Yang<sup>3</sup>, Zheng Liu<sup>4</sup>, Bo Zhao<sup>1</sup>

<sup>1</sup>School of AI, Shanghai Jiao Tong University <sup>2</sup>University of Science and Technology of China

<sup>3</sup>Harbin Institute of Technology (Shenzhen) <sup>4</sup>BAAI

Corresponding to <bo.zhao@sjtu.edu.cn>

## Abstract

*Vision-Language-Action (VLA) models have shown great promise for embodied AI, yet the heavy computational cost of processing continuous visual streams severely limits their real-time deployment. Token pruning—keeping salient visual tokens and dropping redundant ones—has emerged as an effective approach for accelerating Vision-Language Models (VLMs), offering a solution for efficient VLA. However, these VLM-specific token pruning methods select tokens based solely on semantic salience metrics (e.g., prefill attention), while overlooking the VLA’s intrinsic dual-system nature of high-level semantic understanding and low-level action execution. Consequently, these methods bias token retention toward semantic cues, discard critical information for action generation, and significantly degrade VLA performance. To bridge this gap, we propose **VLA-Pruner**, a versatile plug-and-play VLA-specific token prune method that aligns with the dual-system nature of VLA models and exploits the temporal continuity in robot manipulation. Specifically, VLA-Pruner adopts a **dual-level importance criterion** for visual token retention: vision-language prefill attention for semantic-level relevance and action decode attention, estimated via temporal smoothing, for action-level importance. Based on this criterion, VLA-Pruner proposes a novel **dual-level token selection strategy** that adaptively preserves a compact, informative set of visual tokens for both semantic understanding and action execution under given compute budget. Experiments show that VLA-Pruner achieves state-of-the-art performance across multiple VLA architectures and diverse robotic tasks.*

## 1. Introduction

Recent advances in robot learning have led to remarkable progress in developing generalist policies capable of acting across diverse tasks and environments [4, 7, 9, 13, 22, 25, 35, 62, 63]. Vision-Language-Action (VLA) models [4, 7, 22, 23, 25, 30, 63], which benefit from the multimodal understanding and transfer ability of Vision-Language Mod-

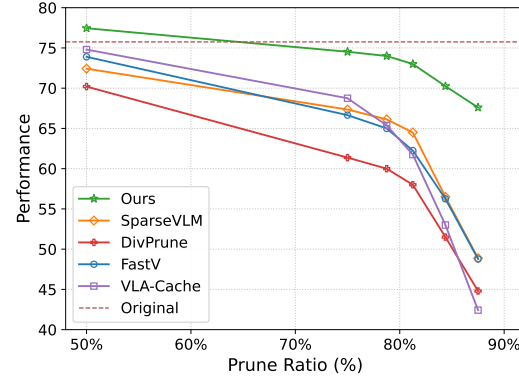


Figure 1. Comparison of different visual token pruning/caching methods across various pruning/caching ratios for OpenVLA [22]. The y-axis is the success rate averaged on the LIBERO [32] benchmark. The proposed method significantly outperforms all baselines, especially at high pruning/caching ratios. At 50% ratio, our method can even improve performance of OpenVLA.

els (VLMs) [3, 33], have emerged as a promising pathway toward general-purpose robot policy. Leveraging large-scale real-world robotic datasets [40], VLA models can perceive visual scenes, understand natural language instructions, and directly execute low-level actions to complete complex tasks across diverse scenarios. However, in real-time deployment, VLA models must process continuous visual streams within dynamic environments and thus struggle with heavy computational overhead. To mitigate this, existing works have explored acceleration techniques such as model lightweighting [51], quantization [41], and early-exit [59] for VLA. Despite effectiveness to some extent, these methods require either architectural modifications or retraining, therefore hindered by poor generalizability.

Previous research [2, 8, 47] has shown that visual representations (i.e., visual tokens) in Vision-Language Models (VLMs) are highly redundant. Consequently, visual token pruning, which retains the most salient tokens while pruning the rest, has become a general and effective approach to improve VLM inference efficiency [2, 8, 47, 53, 57, 60, 64] and shows promise for general VLA acceleration. These

methods typically define *importance criteria* for tokens, such as attention scores [8, 60, 64], gradient information [36, 37] or feature diversity [2] to quantify the significance of visual tokens, and less important tokens are pruned at inference time. By reducing visual redundancy, they yield substantial compute savings with minimal accuracy loss on standard VLM tasks such as image captioning [1, 44], VQA [20, 34], and video understanding [28, 54].

Despite recent progress, existing token pruning methods typically rely solely on *semantic salience* metrics measured during context prefilling—e.g., prefill attention distributions in FastV [8] or text-to-vision cross-attention scores in SparseVLM [60]—to rank visual tokens and prune the lowest-scoring ones. While such semantic-only criteria can be effective for VLMs, they are misaligned with the intrinsic *dual-system nature* of VLA models [11, 18, 19, 48]. Specifically, VLA inference couples high-level semantic understanding, task planning with low-level action execution, which entails distinct visual requirements between its *vision-language prefill* and *action decode* stages; correspondingly, we observe clearly *different attention patterns* across these two stages (see Sec. 3.2). Consequently, current methods tend to bias token retention towards semantic cues, thereby discarding critical details for action generation and significantly degrading VLA performance, especially at high pruning ratios (see Fig. 1), as also observed in prior work [55]. Thus, existing VLM-specific token pruning strategies are fundamentally *ill-suited* for VLA models, highlighting the need for a VLA-specific method.

To bridge this gap, we propose **VLA-Pruner**, a versatile plug-and-play VLA token pruning approach that aligns with the dual-system nature of VLA models and exploits temporal continuity in robot manipulation. VLA-Pruner offers two principal insights for VLA token pruning. First, VLA-Pruner adopts a **dual-level importance criterion** for visual token retention: vision-language prefill attention scores to quantify semantic-level relevance (following prior works [8, 37, 57, 60]), and action decode attention scores to quantify action-level importance. A critical challenge to achieve this is that decode attention is unavailable at prefill time. Fortunately, we observe that *temporal continuity* of robot manipulation [55] manifests in VLA action attention patterns evolving: top-attended visual patches overlap substantially across consecutive timesteps (see Sec. 3.2). Leveraging this continuity, we practically estimate the current action-to-vision attention from recent decode attentions via statistical temporal smoothing techniques (e.g., Exponential Moving Average [14, 15]). Second, to ensure VLA performance, our novel **dual-level token selection strategy** avoids fragile attention score fusion that incurs redundancy and bias. Instead, drawing on the *minimal-redundancy-maximal-relevance* (mRMR) principle [42], we adopt a patch-wise scheme: we first take the union of

patches salient at either semantic or action level to maximize relevance, and then filter them by reducing redundancy, yielding a compact yet informative visual token set that meets the given compute budget. This innovative design reduces computational overhead and adaptively preserves essential information for both semantic understanding and action execution. **VLA-Pruner** is training-free, serving as a plug-and-play acceleration module for most state-of-the-art VLA architectures [4, 22, 24]. We evaluate VLA-Pruner on robotic manipulation across two simulated environments (LIBERO [32] and SIMPLER [27]) and three VLA models (OpenVLA [22], OpenVLA-OFT [24], and  $\pi_0$  [4]). VLA-Pruner delivers substantial efficiency gains (up to  $1.8\times$  speedup) with minor drops in task success rate. Even at 87.5% prune ratio, VLA-Pruner can maintain reasonable performance. Moreover, thanks to precise redundancy removal, VLA-Pruner can **improve model performance** at the 50% prune ratio. Finally, we demonstrate its real-world applicability by deploying it on a 6-DoF xArm6 robot, achieving practical speedups in real-time scenarios.

## 2. Related Work

### 2.1. Vision-Language-Action Models (VLA)

Large-scale vision-language models (VLMs) have propelled multimodal learning by incorporating visual perception and language reasoning [26]. Building on these advances, Vision-Language–Action (VLA) models [4, 7, 22, 24, 63] introduce an action modality, enabling end-to-end motor control. These models typically adopt large VLM backbones [49] and are fine-tuned on robotic data [40]. For action generation, implementations range from discretizing actions into language-like tokens (e.g., OpenVLA [22]) to attaching diffusion-policy heads (e.g.,  $\pi_0$  [4]), typically relying on *action-to-vision cross-attention* for fine-grained interaction. Despite their effectiveness on robot manipulation tasks such as object retrieval and assembly [27, 32], VLA models remain computationally intensive, hindering real-time deployment on resource-constrained platforms.

### 2.2. Visual Token Pruning for VLMs

Visual token pruning [2, 8, 47, 57, 60] is a widely adopted strategy to reduce visual redundancy in VLMs. One line of methods defines *semantic importance criteria* to rank and prune visual tokens, e.g., FastV [8] (using early-layer attention), SparseVLM [60] (using text-to-vision cross-attention), DivPrune [2] (using diversity-driven selection), and HoloV [64] (using crop-wise attention and diversity). Another line of *calibration-based* approaches (e.g., FitPrune [57], VTW [31]) select pruning layers/ratios by analyzing model outputs on a calibration set. However, the first line relies mainly on semantic salience and overlooks the action-dependent requirements of VLA, leading to performance drops (see Sec. 3.2). The second line depends on offline calibration that is unfriendly to resource-constrained

VLA deployment and still hinges on semantic salience. These limitations motivate a VLA-specific pruning method.

### 2.3. Training-Free Acceleration for VLA Models

Visual token pruning has recently been integrated into training-free VLA acceleration frameworks [58]. For example, EfficientVLA [58], SP-VLA [29], and SpecPrune-VLA [50] perform structured acceleration that incorporates token pruning. However, these methods still use semantic salience to retain tokens. Thus, they rely on additional modules (e.g., diffusion-feature cache [56], lightweight generation module [29], action-aware controller [50], or layer-reduction [50, 56]) to balance performance and speed, limiting their generalizability and effectiveness. A recent method, VLA-Cache [55], exploits temporal continuity by caching static visual token features, opening a promising direction. However, its cache-based mechanism is less efficient than direct pruning and still depends on text-to-vision cross-attention to preserve task-relevant tokens in a coarse-grained manner. The above limitations stem from overlooking the dual-system nature of VLA models (see Sec. 3.2). In this paper, we show that token pruning can achieve significant VLA acceleration without sacrificing performance.

## 3. Preliminary Analysis

### 3.1. Background

**VLA Inference.** Vision-Language-Action (VLA) models process sequential inputs of the form  $\{V^t, L^t\}$  into  $A^t$  across timesteps  $t$ . Here,  $V^t$  represents the input visual observations,  $L^t$  denotes language task instructions, and  $A^t = \{a_1^t, \dots, a_{\hat{N}}^t\}$  denotes the predicted action tokens, which can be detokenized into executable robotic actions. The text input is tokenized into  $N$  text tokens  $\mathbf{E}_\tau^t = \{\tau_1^t, \dots, \tau_N^t\}$ . The vision encoder processes  $V^t$  into image features, which are projected into  $M$  visual tokens  $\mathbf{E}_v^t = \{v_1, \dots, v_M\}$  using a projector. These tokens, along with a proprioceptive token representing robot state, form the Transformer input. Since self-attention scales quadratically with token count, the  $M$  (generally  $M \gg N$ ) visual tokens dominate inference cost.

**VLA Attention Breakdown.** Like VLMs, VLA models rely on the attention mechanism of transformer for token interactions. Without loss of generality, we describe the single-head attention below. At each layer  $l$ , the model takes previous-layer hidden states of visual tokens  $\mathbf{H}_v^{l-1} \in \mathbb{R}^{M \times d}$  and textual tokens  $\mathbf{H}_\tau^{l-1} \in \mathbb{R}^{N \times d}$  as inputs. *For mathematical simplicity, we omit time/layer superscripts and treat the proprioceptive token as part of the vision-language context.* These inputs are transformed into queries  $\mathbf{Q}$ , keys  $\mathbf{K}$ , and values  $\mathbf{V}$  using linear projections. Then, the shared vision-language context for attention and interaction is formed as:  $\mathbf{K}_{\text{vl}} \in \mathbb{R}^{(N+M) \times d_k}$ ,  $\mathbf{V}_{\text{vl}} \in \mathbb{R}^{(N+M) \times d_v}$ . We break down VLA inference into two stages:

**(1) Vision-Language prefill Stage.** In this stage, queries

come from the text and vision tokens:  $\mathbf{Q}_{\text{vl}} \in \mathbb{R}^{(N+M) \times d_k}$ . The attention matrix is computed by

$$\mathcal{A}_{\text{vl}} = \text{Softmax} \left( \frac{\mathbf{Q}_{\text{vl}} \mathbf{K}_{\text{vl}}^\top}{\sqrt{d_k}} \right). \quad (1)$$

Attention score for each input visual patch is computed as

$$\mathcal{S}_{\text{vl}}[m] = \frac{1}{M+N} \sum_{i=1}^{M+N} \mathcal{A}_{\text{vl}}[i, m], \quad m = 1, \dots, M. \quad (2)$$

**(2) Action decode Stage.** In this stage, queries are action tokens  $\mathbf{Q}_{\text{act}} \in \mathbb{R}^{K \times d_k}$  ( $K = 1$  for autoregressive [22],  $K = \hat{N}$  for chunk-based [4]). Attention is computed as

$$\mathcal{A}_{\text{act}} = \text{Softmax} \left( \frac{\mathbf{Q}_{\text{act}} \mathbf{K}_{\text{vl}}^\top}{\sqrt{d_k}} \right). \quad (3)$$

For the autoregressive case, attention vectors from  $\hat{N}$  decoding steps are concatenated into the final attention matrix. The action-to-vision attention score in this stage is

$$\mathcal{S}_{\text{act}}[m] = \frac{1}{\hat{N}} \sum_{i=1}^{\hat{N}} \mathcal{A}_{\text{act}}[i, m], \quad m = 1, \dots, M. \quad (4)$$

$\mathcal{S}_{\text{vl}}$  and  $\mathcal{S}_{\text{act}}$  quantifies each patch’s significance to semantic understanding [55, 60] and action execution, respectively.

### 3.2. Motivating Observation for VLA-Pruner

We systematically delve into the intrinsic characteristics of VLA inference (Fig. 2). Our findings identify the fundamental limitations of current VLM-specific token pruning methods for VLA models, which motivate our VLA-Pruner.

**Motivation 1: Visual token prefilling dominates computational overhead for VLA models.** As noted in previous works [8, 60], incorporation of visual tokens inevitably introduces substantial memory and computational overhead when compared to LLMs. For VLA models, the number of processed visual tokens (typically  $256 \times n$  per frame, where  $n$  is the number of camera views) is often an order of magnitude larger than that of text tokens ( $\sim 30\text{--}50$ ) and action tokens ( $\sim 7\text{--}56$ ), making input visual stream prefilling the primary contributor to the computational cost. Since visual representations are highly redundant [2, 8, 60], visual token pruning shows great promise for VLA acceleration.

**Motivation 2: Visual token pruning must account for the dual-system nature of VLA models.** The efficacy of VLA models stems from their inherent dual-system ability to integrate high-level semantic understanding and task planning with low-level action execution [11, 13, 18, 19, 48]. Our key insight is that this inherent duality manifests directly in VLA model inference, resulting in distinct visual requirements for its two stages: vision-language prefill and action decode. To investigate this, we analyzed the attention distributions of OpenVLA [22] on the LIBERO benchmark [32] (Fig. 2). The results reveal that VLA inference

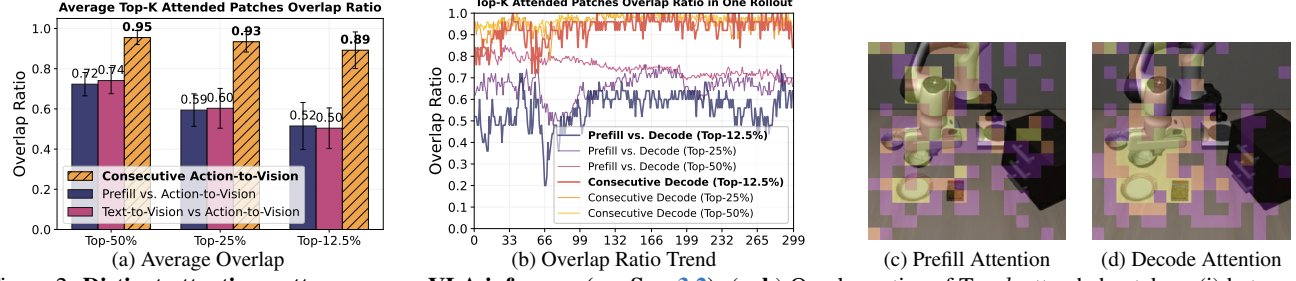


Figure 2. **Distinct attention patterns across VLA inference** (see Sec. 3.2). (a–b) Overlap ratios of Top- $k$  attended patches: (i) between vision–language prefill and action decode (Top- $k$ ( $\mathcal{S}_{\text{vl}}$ ) vs. Top- $k$ ( $\mathcal{S}_{\text{act}}$ )), and (ii) between consecutive action-decode timesteps (Top- $k$ ( $\mathcal{S}_{\text{act}}^t$ ) vs. Top- $k$ ( $\mathcal{S}_{\text{act}}^{t-1}$ )). We show the average values (a) and a representative rollout (b). (c–d) Visualization of prefill (c) and action decode (d) attention over the same frame; top 12.5% (yellow), 25% (orange), and 50% (purple) patches are overlaid. Prefilling shows broad semantic coverage, while action decoding is locally focused. The results reveal VLA model’s **dual-system nature** that token pruning must consider.

demonstrates **distinct attention patterns**: prefill attention exhibits a broad, semantic distribution, while action decode attention shows localized focus essential for precise motor control, as exemplified in Fig. 2c and Fig. 2d. Quantitatively, the overlap ratio of top-attended visual tokens between vision–language prefilling and action decoding averages  $\sim 50\%$  and often falls below 30% (Fig. 2). Attention scores are averaged across all Transformer layers. Existing pruning strategies overlook this crucial attention divergence, thereby risking the premature removal of tokens vital for action generation but less salient during prefilling, particularly at high compression ratios. This oversight is critical, since removing even a few high-attention tokens is known to severely degrade performance [16, 61]. We also provide a qualitative illustration in Fig. 7.

**Motivation 3: VLA token pruning should exploit temporal continuity in robotic manipulation.** Since vision token prefilling dominates computational overhead (Motivation 1), token pruning must operate during early-layer prefilling [8]. However, while an ideal strategy should consider both semantic and action-level token importance (Motivation 2), action decode attention scores (practical proxy for action-level importance) are unavailable at prefill time. Fortunately, VLA robot manipulation exhibits *temporal continuity* [55]. We observe that action-to-vision attention maps show strong short-term temporal correlation: the top-attended visual tokens during action decoding at timesteps  $t$  and  $t-1$  show consistently high overlap ratios (Fig. 2 show ratios averaged across LIBERO tasks and a representative rollout). This temporal continuity makes statistical temporal smoothing techniques [14, 21, 52] an practical and effective proxy for estimating current action-to-vision attention.

## 4. Methodology

### 4.1. Problem Formulation

We define the token pruning problem as follows: given a set of visual tokens  $\mathbf{E}_v$  with  $|\mathbf{E}_v| = M$  and a target subset size  $\tilde{M} < M$ , the goal is to select a subset  $\tilde{\mathbf{E}}_v$  that preserves information critical for VLA inference. Formally, we define

a mapping  $f$  that selects an index subset  $\tilde{\mathcal{I}} \subseteq \{1, \dots, M\}$  with  $|\tilde{\mathcal{I}}| = \tilde{M}$ , and constructs the retained visual tokens as  $\tilde{\mathbf{E}}_v = f(\mathbf{E}_v) = \{\mathbf{E}_v[i] : i \in \tilde{\mathcal{I}}\}$ . The objective is to identify a mapping function  $f$  that minimizes the difference in the model’s output before and after pruning:

$$\begin{aligned} \text{Find: } & f : \mathbf{E}_v \rightarrow \tilde{\mathbf{E}}_v \\ \text{Objective: } & \min_f \mathcal{L}(\mathcal{P}, \tilde{\mathcal{P}}) \\ \text{Subject to: } & |\tilde{\mathbf{E}}_v| = \tilde{M}, \end{aligned} \quad (5)$$

where  $\mathcal{P} = P(A \mid \mathbf{E}_\tau, \mathbf{E}_v)$  and  $\tilde{\mathcal{P}} = P(A \mid \mathbf{E}_\tau, f(\mathbf{E}_v))$ .  $P(\cdot)$  denotes the conditional generation probability of VLA model.  $\mathcal{L}$  denotes a loss function that measures the difference in the model’s output with and without pruning, and  $\tilde{M}$  indicates the number of retained tokens. We conceptually decompose  $\mathcal{P}$  into vision-language prefill  $P_{\text{vl}}$  and action decode  $P_{\text{act}}$ . Let  $\mathbf{Z}_\tau, \mathbf{Z}_v$  denote all hidden representations of textual and visual tokens after prefilling. Informally,

$$\begin{aligned} \mathcal{P} &= P_{\text{vl}}(\mathbf{Z}_\tau, \mathbf{Z}_v \mid \mathbf{E}_\tau, \mathbf{E}_v) \cdot P_{\text{act}}(A \mid \mathbf{Z}_\tau, \mathbf{Z}_v), \\ \tilde{\mathcal{P}} &= \tilde{P}_{\text{vl}}(\tilde{\mathbf{Z}}_\tau, f(\tilde{\mathbf{Z}}_v) \mid \mathbf{E}_\tau, f(\mathbf{E}_v)) \cdot \tilde{P}_{\text{act}}(A \mid \tilde{\mathbf{Z}}_\tau, f(\tilde{\mathbf{Z}}_v)), \end{aligned}$$

where  $f$  also drops the corresponding indices from the hidden visual representations  $\tilde{\mathbf{Z}}_v$ . As noted in Motivation 2, optimizing  $f$  with a single-level objective, i.e., semantic-level  $\mathcal{L}(P_{\text{vl}}, \tilde{P}_{\text{vl}})$  or action-level  $\mathcal{L}(P_{\text{act}}, \tilde{P}_{\text{act}})$ , leads to sub-optimal pruning. To address this, we propose VLA-Pruner.

### 4.2. The Proposed VLA-Pruner

VLA-Pruner adopts a **(a) dual-level token importance criterion** that incorporates both semantic-level and action-level importance for visual token retention, and proposes a corresponding **(b) dual-level token selection strategy** to adaptively process dual-level relevance and redundancy for token retention. The overall pipeline is illustrated in Fig. 3.

#### (a) Dual-level Token Importance Criterion

For VLMs, previous works [8, 60] have demonstrated that prefill or text-to-vision attention scores can effectively quantify significance of vision tokens. In VLA case, as discussed before (Sec. 3.2), both semantic-level and action-

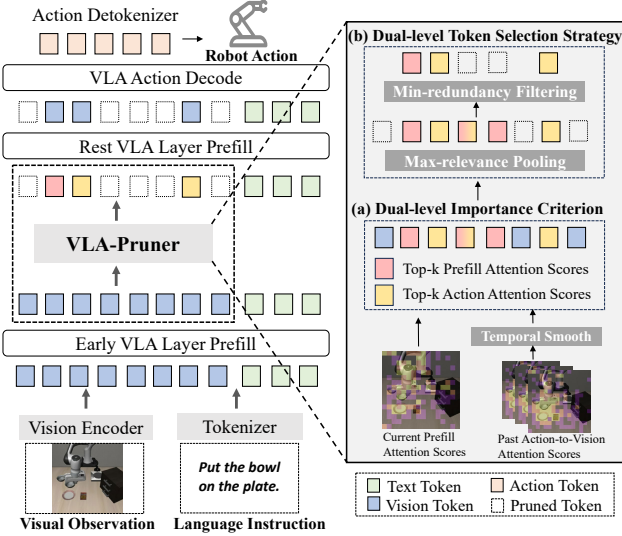


Figure 3. **Overall pipeline of VLA-Pruner** illustrated with token budget  $k=3$ . It adopts (a) **dual-level token importance criterion** that incorporates semantic-level and action-level importance and (b) **dual-level token selection strategy** that combines max-relevance and min-redundancy principle. See Sec. 4.2 for details.

level visual requirements should be satisfied. To this end, VLA-Pruner adopts a dual-level token importance criterion: (1) prefill attention scores  $\mathcal{S}_{\text{vl}}^t$  (Eq. 2) to quantify semantic-level relevance and (2) action decode attention scores  $\mathcal{S}_{\text{act}}^t$  (Eq. 3) to quantify action-level importance. As discussed in Motivation 3, we build on the **temporal continuity** of VLA manipulation to estimate current action attention scores  $\hat{\mathcal{S}}_{\text{act}}^t$  over image patches. This formulates a **time-series forecasting task** [5], where  $\mathcal{S}_{\text{act}}^t$  is estimated from historical trend  $\{\mathcal{S}_{\text{act}}^{t-1}, \mathcal{S}_{\text{act}}^{t-2}, \dots\}$ . Classical training-free forecasting methods include averaging, autoregressive models, and exponential smoothing [5, 6, 52]. Among them, the Exponential Moving Average (EMA) [14, 15, 21] provides a simple yet effective way to estimate temporal trends. By emphasizing recent observations while discounting older ones, EMA reduces noise, captures temporal trends, and has been widely applied in domains such as finance, economics, meteorology, and robotic manipulation [10, 17, 39, 43]. Directly applying EMA to our task takes this form:

$$\hat{\mathcal{S}}_{\text{act}}^t = (1 - \alpha)\hat{\mathcal{S}}_{\text{act}}^{t-1} + \alpha\mathcal{S}_{\text{act}}^{t-1} \quad (6)$$

where  $\alpha \in [0, 1]$  is the smoothing factor,  $\hat{\mathcal{S}}_{\text{act}}^{t-1}$  denotes the smoothed prediction at the previous timestep, and  $\mathcal{S}_{\text{act}}^{t-1}$  represents the corresponding observation result.

**Decaying Window Average Mechanism.** For VLA manipulation, where short-term context is more critical [55], we instead propose a simpler and more intuitive decaying window average mechanism. This method considers recent  $w$  timesteps and applies an explicit exponential decay. Formally, we smooth action attention scores from previous  $w$  steps,  $\{\mathcal{S}_{\text{act}}^{t-1}, \dots, \mathcal{S}_{\text{act}}^{t-w}\}$ , and compute the estimated score

for current step  $\hat{\mathcal{S}}_{\text{act}}^t$  as their weighted sum:

$$\hat{\mathcal{S}}_{\text{act}}^t = \sum_{i=1}^w \gamma^i \mathcal{S}_{\text{act}}^{t-i} \quad (7)$$

where  $w$  defines the window size, and  $\gamma \in [0, 1]$  controls the decay rate. This formulation provides a simple yet effective mechanism to estimate current action attention scores. For brevity, we omit time superscript  $t$  in following discussion.

**Remark 1.** *Temporal smoothing methods can reliably estimate action attention dynamic trends but may fail under abrupt changes, such as target switching. For instance, in the LIBERO-Long task “put both the alphabet soup and the tomato sauce in the basket”, action attention from putting the soup does not ground the tomato sauce well. Potential remedies include lightweight predictors for attention shifts or mechanisms to bypass pruning when large prediction–observation discrepancies occur. To ensure generalizability and flexibility, we instead tackle this fundamental challenge through our dual-level token selection strategy.*

### (b) Dual-Level Token Selection Strategy.

Based on the dual-level token importance criterion, an intuitive approach to retain tokens is: normalizing semantic and action attention scores ( $\mathcal{S}_{\text{vl}}$  and  $\hat{\mathcal{S}}_{\text{act}}$ ), taking a weighted sum, and selecting the top- $\tilde{M}$  tokens by the weighted score. However, this scheme suffers from fundamental limitations. First, it introduces a sensitive weighting hyperparameter that must be carefully tuned, compromising robustness and generalizability. Second, it ignores redundancy both within and across stages. On one hand, as noted in prior work [2], attention-based pruning often retains similar tokens. On the other hand, score-level fusion tends to retain tokens that appear salient in both prefilling and decoding, yet not essential to either stage. For example, in a robotic arm, intermediate arm segments may appear salient across both stages, whereas the end-effector (critical for execution) can be undervalued. Finally, it implicitly assumes that the action attention estimate  $\hat{\mathcal{S}}_{\text{act}}$  is always reliable, which may not hold under abrupt attention shifts (see Remark 1).

**Patch-wise Combine-then-Filter.** To avoid these limitations, we draw on the *minimal-Redundancy-Maximal-Relevance* (mRMR) principle [42], an information-theoretic paradigm for feature selection. mRMR proposes to combine both Max-Relevance and Min-Redundancy principles, reducing the redundant features while keeping the relevant features for the task. Inspired by this, our dual-level token selection strategy follows a patch-wise *combine-then-filter* mechanism. We organize the procedure into three phases: **(1) Dual-level Top-k Selection.** We begin by constructing two candidate token subsets via dual-level top-k selection:

$$\mathcal{C}_{\text{vl}} = \text{Top-}\tilde{M} \left( \{\mathcal{S}_{\text{vl}}[i]\}_{i=1}^M \right), \mathcal{C}_{\text{act}} = \text{Top-}\tilde{M} \left( \{\hat{\mathcal{S}}_{\text{act}}[i]\}_{i=1}^M \right),$$

where  $\tilde{M}$  is the target token budget. This phase identifies salient tokens (indices) for high-level semantic understanding ( $\mathcal{C}_{\text{vl}}$ ) and low-level action execution ( $\mathcal{C}_{\text{act}}$ ), respectively.

**(2) Relevance-Maximization Pooling.** We then combine these two subsets to form a candidate pool:

$$\mathcal{C}_{\text{dual}} = \mathcal{C}_{\text{vl}} \cup \mathcal{C}_{\text{act}}.$$

This subset  $\mathcal{C}_{\text{dual}}$  constructs a candidate pool that contains tokens essential for dual-level information requirements, maximizing two-stage task relevance. Due to attention divergence (Motivation 2),  $|\mathcal{C}_{\text{dual}}|$  is generally larger than  $\tilde{M}$ .

**(3) Redundancy-Minimization Filtering.** This phase aims to reduce feature redundancy within the candidates  $\mathcal{C}_{\text{dual}}$  to satisfy the target budget  $\tilde{M}$ . We achieve this by maximizing the diversity of the final selected subset. Following prior work [2], we formulate it as a Max–Min Diversity Problem (MMDP) [45] within candidate pool  $\mathcal{C}_{\text{dual}}$ , where the goal is to find a subset  $\tilde{\mathcal{C}} \subset \mathcal{C}_{\text{dual}}$  of size  $\tilde{M}$  that maximizes the minimum pairwise distance between its elements:

$$\tilde{\mathcal{C}} = \arg \max \left[ \min_{i, j \in \mathcal{C}} d(v_i, v_j) : \forall \mathcal{C} \subset \mathcal{C}_{\text{dual}}, |\mathcal{C}| = \tilde{M} \right], \quad (8)$$

where  $\mathcal{C}$  is any subset of  $\mathcal{C}_{\text{dual}}$  with  $\tilde{M}$  elements, and  $v_i, v_j \in \mathbf{E}_v$  are input image patch embeddings indexed by any  $i, j \in \mathcal{C}$ . The distance  $d(\cdot, \cdot)$  is defined as the cosine distance:

$$d(v_i, v_j) = 1 - \frac{v_i \cdot v_j}{\|v_i\| \|v_j\|}. \quad (9)$$

A solution for the MMDP problem 4.2 is a subset of  $\mathcal{C}_{\text{dual}}$  that minimizes redundancy between elements. MMDP can be solved by several exact and heuristic methods [38, 46]. To facilitate efficiency, we use a greedy algorithm that iteratively add tokens whose minimum distance to the retained set is maximal, until reaching  $\tilde{M}$  elements. To escape local optima, we initialize the first token with maximal second-nearest distance. We detail the step (3) and our overall token selection method in Algorithm 1 and 2 (see Appendix A).

**Remark 2.** Our method is a heuristic solution for mRMR objective: the first two steps maximize task relevance, while the final step minimizes feature redundancy. The challenge in Remark 1 is addressed by grounding abrupt shifts by prefill attention and retaining them via diversity maximization.

**Remark 3.** Step (3) shares similarities with DivPrune [2], which reduces redundancy through diversity-based pruning. However, DivPrune does not incorporate relevance maximization step, thus fail to identify pivotal tokens. By combining both Max-relevance and Min-redundancy, we retain token subsets that are both diverse and better matched to dual-level information requirements within VLA inference.

### (c) Implementation Details.

VLA-Pruner prunes visual tokens at Transformer layer K within VLA model (K is set to 3 [8]). We select tokens

using last-layer prefill attention and temporal smoothing of action-to-vision attention averaged over the latter half layers (to reduce noise) from past timesteps. Pruned tokens are dropped from the rest prefill layers. To adapt to flash-attention [12], adaptation techniques in SparseVLM [60] can be adopted. For decaying window average, window size  $w$  and decay rate  $\gamma$  are empirically set as 3 and 0.8. We warm-start VLA-Pruner with  $w$  steps to record sufficient action attention history. VLA-Pruner is a plug-and-play acceleration module for VLA architectures with action-to-vision cross-attention, a mechanism used by state-of-the-art VLA models [4, 22, 24], including (i) autoregressive policies [7, 22, 63, 63] (e.g., OpenVLA [22]), (ii) action-chunk decoders (OpenVLA-OFT [24]), and (iii) diffusion-head policies such as  $\pi_0$  [4], for which we average action attention scores over its flow-matching steps. We provide analysis of computational complexity in Appendix A.2.

## 5. Experiments

We evaluate VLA-Pruner in both simulation and real-world settings. In simulation setting, we evaluate VLA-Pruner on open-source VLA models: OpenVLA [22], OpenVLA-OFT [24] and  $\pi_0$  [4], using the LIBERO benchmark [32] and SIMPLER environment [27]. All experiments are conducted on an NVIDIA RTX 4090 GPU.

### 5.1. Experimental Setup

**Baselines.** We compare VLA-Pruner with a comprehensive suite of training-free accelerators under given compute budgets. Baselines include state-of-the-art token pruning methods (FastV [8], SparseVLM [60], and DivPrune [2]) and a VLA-specific method VLA-Cache [55]. We provide more details of baselines and VLA models in Appendix B.1. EfficientVLA [56] adopts token prune strategies similar to prior work (using attention and diversity), we include results of it and more token pruning baselines in Appendix B.3.

**Evaluation Protocol.** All methods are evaluated under identical given pruning budgets. To ensure a comprehensive comparison, our experiments include diverse pruning ratios (50%, 75%, 87.5%). For VLA-Cache, we set the same token reuse ratio. Our evaluation metrics mainly include: task success rate (%), inference latency (ms) and FLOPs(T).

### 5.2. Evaluation Benchmarks

In this section, we introduce the evaluation benchmarks, with more details presented in Appendix B.2.

**LIBERO.** The LIBERO benchmark [32] comprises four suites (*Spatial*, *Object*, *Goal*, and *Long*) that probe complementary aspects of manipulation generalization. Each suite contains 10 distinct tasks with 50 evaluation episodes per task (500 total episodes per suite). Following OpenVLA [22] and OpenVLA-OFT [24], we adopt their standard evaluation setup (action chunks as 8 for OpenVLA-OFT) and official weights to ensure comparability. To verify cross-architecture generality, we also include results of diffusion-head based model  $\pi_0$  [4].(see Appendix B.4)

Table 1. **Performance of VLA-Pruner on OpenVLA and OpenVLA-OFT across LIBERO** at 50%, 25%, and 12.5% vision-token retention. Vanilla visual tokens: 256 (OpenVLA), 512 (OpenVLA-OFT). For each method, the first line shows average success rates(%) on *Spatial/Object/Goal/Long*; the second line shows relative accuracy vs. vanilla (100%) or speedup ratio ( $\times$ ). We also report FLOPs (T), inference latency (ms/action; ms/action-chunk).

| Method   | OpenVLA        |                |                |                |                                       |                       |                          | OpenVLA-OFT    |               |                |                |                                       |                       |                          |
|--|----------------|----------------|----------------|----------------|---------------------------------------|-----------------------|--------------------------|----------------|---------------|----------------|----------------|---------------------------------------|-----------------------|--------------------------|
|  | Spatial        | Object         | Goal           | Long           | Acc.(%) $\uparrow$                    | FLOPs(T) $\downarrow$ | Latency(ms) $\downarrow$ | Spatial        | Object        | Goal           | Long           | Acc.(%) $\uparrow$                    | FLOPs(T) $\downarrow$ | Latency(ms) $\downarrow$ |
| <i>Upper Bound (100%)</i>                                  |                |                |                |                |                                       |                       |                          |                |               |                |                |                                       |                       |                          |
| Vanilla  | 87.6<br>100%   | 84.6<br>100%   | 78.6<br>100%   | 52.2<br>100%   | 100.0<br>( $\rightarrow$ )            | 1.906<br>100.00%      | 236.41<br>1.00 $\times$  | 95.8<br>100%   | 98.7<br>100%  | 96.3<br>100%   | 90.7<br>100%   | 100.0<br>( $\rightarrow$ )            | 3.903<br>100%         | 135.78<br>1.00 $\times$  |
| <i>Retain 50% Tokens (<math>\downarrow</math> 50%)</i>     |                |                |                |                |                                       |                       |                          |                |               |                |                |                                       |                       |                          |
| FastV  | 86.2<br>98.4%  | 81.6<br>96.5%  | 77.2<br>98.2%  | 50.6<br>96.9%  | 97.43<br>( $\downarrow$ 2.57)         | 1.136<br>59.60%       | 172.32<br>1.37 $\times$  | 94.6<br>98.7%  | 96.8<br>98.1% | 92.7<br>96.3%  | 87.0<br>95.9%  | 97.26<br>( $\downarrow$ 2.74)         | 2.219<br>56.85%       | 88.23<br>1.54 $\times$   |
| SparseVLM  | 85.6<br>97.7%  | 80.5<br>95.2%  | 75.0<br>95.4%  | 48.6<br>93.1%  | 95.44<br>( $\downarrow$ 4.56)         | 1.155<br>60.60%       | 175.77<br>1.34 $\times$  | 94.1<br>98.3%  | 93.7<br>94.9% | 91.2<br>94.7%  | 85.1<br>93.8%  | 95.37<br>( $\downarrow$ 4.63)         | 2.289<br>58.65%       | 90.22<br>1.50 $\times$   |
| DivPrune   | 82.6<br>94.3%  | 78.8<br>93.1%  | 71.8<br>91.3%  | 47.6<br>91.2%  | 92.64<br>( $\downarrow$ 7.36)         | 1.105<br>57.97%       | 173.88<br>1.36 $\times$  | 90.8<br>94.8%  | 91.1<br>92.3% | 89.9<br>93.3%  | 83.1<br>91.7%  | 92.61<br>( $\downarrow$ 7.39)         | 2.126<br>54.47%       | 88.01<br>1.54 $\times$   |
| VLA-Cache  | 87.1<br>99.4%  | 80.7<br>95.4%  | 78.6<br>100.0% | 51.8<br>99.2%  | 98.48<br>( $\downarrow$ 1.52)         | 1.384<br>72.61%       | 192.20<br>1.23 $\times$  | 95.4<br>99.6%  | 96.0<br>97.3% | 96.7<br>100%   | 90.2<br>99.4%  | 99.09<br>( $\downarrow$ 0.91)         | 2.730<br>69.95%       | 101.01<br>1.34 $\times$  |
| <b>VLA-Pruner</b>  | 88.2<br>100.7% | 85.8<br>101.4% | 79.4<br>101.0% | 56.4<br>108.0% | <b>102.45</b><br>( $\uparrow$ 2.45)   | 1.139<br>59.76%       | 178.38<br>1.33 $\times$  | 97.3<br>101.6% | 98.6<br>99.9% | 96.8<br>100.5% | 92.6<br>102.1% | <b>101.05</b><br>( $\uparrow$ 1.05)   | 2.234<br>57.24%       | 92.86<br>1.46 $\times$   |
| <i>Retain 25% Tokens (<math>\downarrow</math> 75%)</i>     |                |                |                |                |                                       |                       |                          |                |               |                |                |                                       |                       |                          |
| FastV  | 81.6<br>93.2%  | 69.6<br>82.3%  | 71.6<br>91.1%  | 43.8<br>83.9%  | 87.62<br>( $\downarrow$ 12.38)        | 0.757<br>39.72%       | 141.25<br>1.67 $\times$  | 87.8<br>91.7%  | 81.8<br>82.9% | 87.6<br>91.0%  | 74.6<br>82.3%  | 87.48<br>( $\downarrow$ 12.52)        | 1.401<br>35.89%       | 72.73<br>1.87 $\times$   |
| SparseVLM  | 83.4<br>95.2%  | 72.8<br>86.1%  | 67.6<br>86.0%  | 45.6<br>87.4%  | 88.67<br>( $\downarrow$ 11.33)        | 0.772<br>40.50%       | 144.12<br>1.64 $\times$  | 89.8<br>93.7%  | 84.8<br>85.9% | 82.7<br>85.9%  | 79.1<br>87.2%  | 88.63<br>( $\downarrow$ 11.37)        | 1.459<br>37.38%       | 74.71<br>1.82 $\times$   |
| DivPrune   | 77.4<br>88.4%  | 61.3<br>72.5%  | 65.4<br>83.2%  | 41.4<br>79.3%  | 80.96<br>( $\downarrow$ 19.04)        | 0.743<br>38.98%       | 142.12<br>1.66 $\times$  | 83.9<br>87.6%  | 72.6<br>73.6% | 79.3<br>82.3%  | 72.5<br>79.9%  | 80.76<br>( $\downarrow$ 19.24)        | 1.389<br>35.58%       | 72.30<br>1.88 $\times$   |
| VLA-Cache  | 78.1<br>89.2%  | 73.2<br>86.5%  | 70.2<br>89.3%  | 45.5<br>87.2%  | 88.08<br>( $\downarrow$ 11.92)        | 0.961<br>50.42%       | 164.17<br>1.44 $\times$  | 85.6<br>89.4%  | 85.3<br>86.4% | 84.1<br>87.3%  | 80.3<br>88.5%  | 88.11<br>( $\downarrow$ 11.89)        | 1.938<br>49.65%       | 85.02<br>1.60 $\times$   |
| <b>VLA-Pruner</b>  | 85.4<br>97.5%  | 82.5<br>97.5%  | 78.4<br>99.7%  | 51.8<br>99.2%  | <b>98.48</b><br>( $\downarrow$ 1.52)  | 0.758<br>39.77%       | 144.81<br>1.63 $\times$  | 93.5<br>97.6%  | 96.2<br>97.5% | 95.2<br>98.9%  | 90.2<br>99.5%  | <b>98.37</b><br>( $\downarrow$ 1.63)  | 1.420<br>36.38%       | 75.64<br>1.80 $\times$   |
| <i>Retain 12.5% Tokens (<math>\downarrow</math> 87.5%)</i> |                |                |                |                |                                       |                       |                          |                |               |                |                |                                       |                       |                          |
| FastV  | 62.0<br>70.8%  | 58.5<br>69.1%  | 55.8<br>71.0%  | 18.8<br>36.0%  | 63.08<br>( $\downarrow$ 36.92)        | 0.568<br>29.80%       | 125.76<br>1.88 $\times$  | 60.6<br>63.3%  | 59.2<br>60.0% | 60.6<br>62.9%  | 28.6<br>31.5%  | 61.64<br>( $\downarrow$ 38.36)        | 1.082<br>27.72%       | 66.11<br>2.05 $\times$   |
| SparseVLM  | 65.8<br>75.1%  | 55.3<br>65.4%  | 55.4<br>70.5%  | 19.0<br>36.4%  | 63.20<br>( $\downarrow$ 36.80)        | 0.581<br>30.48%       | 128.77<br>1.84 $\times$  | 73.1<br>76.3%  | 65.0<br>65.8% | 67.5<br>70.1%  | 32.8<br>36.1%  | 62.11<br>( $\downarrow$ 37.89)        | 1.136<br>29.11%       | 67.65<br>2.01 $\times$   |
| DivPrune   | 55.4<br>63.2%  | 54.8<br>64.8%  | 51.4<br>65.4%  | 17.6<br>33.7%  | 58.06<br>( $\downarrow$ 41.94)        | 0.569<br>29.28%       | 125.36<br>1.89 $\times$  | 61.4<br>64.1%  | 61.8<br>62.6% | 64.9<br>67.4%  | 30.8<br>34.0%  | 56.83<br>( $\downarrow$ 43.17)        | 1.059<br>27.13%       | 66.46<br>2.04 $\times$   |
| VLA-Cache  | 52.5<br>59.9%  | 50.1<br>59.2%  | 52.0<br>66.2%  | 15.1<br>28.9%  | 54.79<br>( $\downarrow$ 45.21)        | 0.710<br>37.25%       | 145.93<br>1.62 $\times$  | 57.3<br>59.8%  | 58.7<br>59.5% | 64.8<br>67.3%  | 26.2<br>28.9%  | 53.88<br>( $\downarrow$ 46.12)        | 1.373<br>35.18%       | 76.15<br>1.78 $\times$   |
| <b>VLA-Pruner</b>  | 80.2<br>91.6%  | 78.4<br>92.7%  | 69.0<br>87.8%  | 42.8<br>82.0%  | <b>88.90</b><br>( $\downarrow$ 11.10) | 0.571<br>29.96%       | 129.01<br>1.83 $\times$  | 88.1<br>91.9%  | 87.6<br>91.7% | 84.9<br>88.1%  | 68.8<br>81.3%  | <b>88.27</b><br>( $\downarrow$ 11.73) | 1.096<br>28.08%       | 68.95<br>1.99 $\times$   |

**SIMPLER.** The SIMPLER simulators [27] provide two complementary settings aimed at closing sim-to-real gaps: visual matching (VM) and variant aggregation (VA). We report evaluation results on three tasks and their corresponding settings: *Move Near*, *Pick Coke Can* (under VA), and *Open/Close Drawer* (under VM). We choose these task-setting pairs where the vanilla OpenVLA attains non-trivial success rates, ensuring a reasonable comparison.

**Real Robot Evaluation.** To assess VLA-Pruner’s performance in real-world scenarios, we conduct experiments using a 6-DoF xArm6 robotic arm equipped with a parallel gripper. We run four manipulation tasks involving diverse objects (100 trials for each task): (1) **Can Stack**: grasp the can and stack it on top of the box; (2) **Cup Pour**: pick up the cup and pour the small balls inside the cup into the box; (3) **Cube Place**: grasp the cube and place it into the box; (4) **Bottle Place**: grasp the bottle and place it into the box.

### 5.3. Main Results

**Results on LIBERO.** We evaluate VLA-Pruner on OpenVLA (fine-tuned) and OpenVLA-OFT for LIBERO benchmark. Table 1 reports *success rate* on the four suites under token-retention ratios of 50%, 25%, and 12.5%. We also report a *relative accuracy* metric that measures pruning-induced error, defined as the performance preservation ratio (vanilla model as 100%). VLA-Pruner achieves the best success rate and relative accuracy across all settings among

| Method            | Move Near        | Pick Coke Can    | Open/Close Drawer | Overall          |
|-------------------|------------------|------------------|-------------------|------------------|
| OpenVLA           | 54.0%<br>(100%)  | 52.8%<br>(100%)  | 49.5%<br>(100%)   | 52.1%<br>(100%)  |
| FastV             | 38.7%<br>(71.7%) | 41.9%<br>(79.4%) | 33.7%<br>(68.1%)  | 38.1%<br>(73.1%) |
| VLA-Cache         | 41.2%<br>(76.3%) | 40.6%<br>(76.9%) | 38.8%<br>(78.4%)  | 40.2%<br>(77.2%) |
| <b>VLA-Pruner</b> | 52.4%<br>(97.0%) | 50.1%<br>(94.9%) | 48.8%<br>(98.6%)  | 50.4%<br>(96.8%) |

Table 2. **Success rates of VLA-Pruner on SIMPLER manipulation tasks and overall performance at 75% token pruning ratio.** We also present performance preservation ratio relative to original OpenVLA.

training-free accelerators. Even at a 12.5% retention ratio, it maintains 88.9% and 88.27% relative accuracy on OpenVLA and OpenVLA-OFT, respectively, outperforming baselines by up to 34.39%. At a 50% retention ratio, VLA-Pruner can even improve success rate, thanks to precise noise filtering that stabilizes policy execution. This is evident on *LIBERO-Long*, where it achieves 4.2% success rate improvement. DivPrune benefits VLM inference but degrades VLA performance since robot manipulation needs more localized visual details. VLA-Cache achieves competitive results due to temporal awareness but fails at high compression ratios because its text-to-vision attention selection strategy is coarse-grained. Fig. 4 visualizes more details of VLA-Pruner performance varying under different pruning ratios. We present results on  $\pi_0$  in Appendix B.4.

**Results on SIMPLER.** We evaluate cross-environment generalization on the SIMPLER environment. Table 2 com-

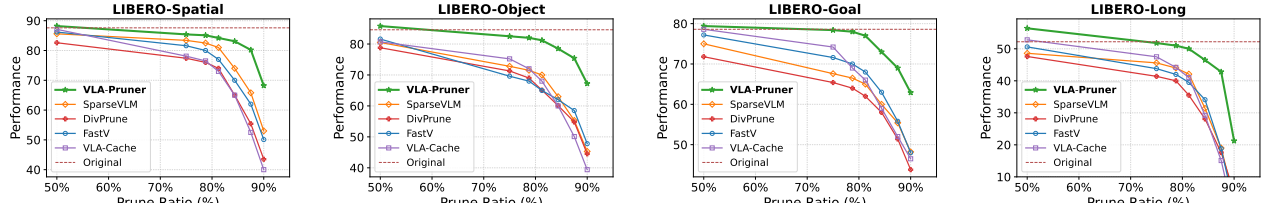


Figure 4. Performance of OpenVLA with pruning/caching methods across LIBERO tasks under varying pruning/caching ratio. The horizontal axis represents the pruning/caching ratios of visual tokens, and the vertical axis shows the success rates. VLA-Pruner performs best, especially as ratio increases.

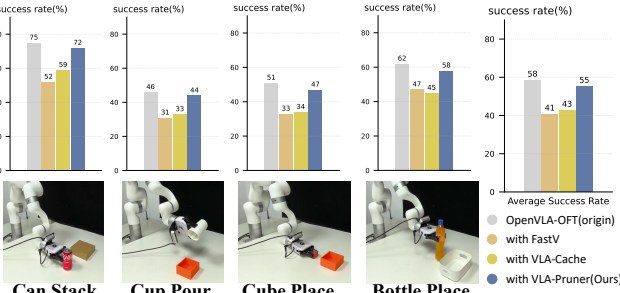


Figure 5. Performance of VLA-Pruner on OpenVLA-OFT for real-robot tasks under a 75% prune ratio. We conduct experiments using a 6-DoF xArm6 robotic arm. VLA-Pruner achieves consistent superiority in preserving model performance, demonstrating its practical advantage.

pares VLA-Pruner with acceleration baselines on OpenVLA at 75% compression ratio. VLA-Pruner best preserves accuracy, showing robust transfer across environments.

**Results on Real Robot.** We evaluate real-world performance on a physical 6-DoF xArm6 arm controlled by OpenVLA-OFT. Fig. 5 reports results under 75% token-pruning ratio. VLA-Pruner attains the highest relative accuracy, underscoring its practicality for on-robot deployment.

**Efficiency Analysis.** We report inference efficiency metrics in Table 1, including inference latency (ms/action or ms/action-chunk) and FLOPs(T). At same pruning ratios, VLA-Pruner achieves comparable speedups to visual token-pruning methods. Its latency is  $\sim 5$  ms higher than FastV (due to distance computations in redundancy filtering), yet it achieves significantly better performance. At the 25% retention ratio, VLA-Pruner outperforms token pruning baselines at 50% retention, while being  $\sim 16\%$  faster and using  $\sim 20\%$  fewer FLOPs. VLA-Pruner is faster and more compute-efficient than VLA-Cache. VLA-Pruner requires storing historical attention, but it introduces a negligible increase in Max GPU memory (see Appendix B.5.1).

#### 5.4. More Results

**Ablation Studies.** To validate our (a) dual-level importance criterion and (b) patch-wise dual-level token selection strategy, we ablate three variants: (1) **prefill-only**, which selects tokens by prefill attention; (2) **action-only**, which selects tokens by action attention; and (3) **score-fusion**, which ranks tokens by the weighted sum of prefill and action attention scores, with a carefully fine-tuned weight. As shown in Fig. 6, *prefill-only* preserves high-level semantics but hinders fine-grained low-level control, whereas *action-only*

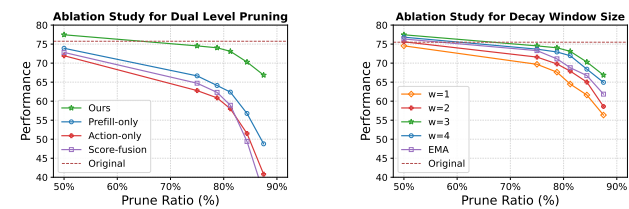


Figure 6. Ablation study to validate our dual-level design and temporal decay window size. We evaluate on OpenVLA with LIBERO. The results substantiate the sound design and robustness of VLA-Pruner.

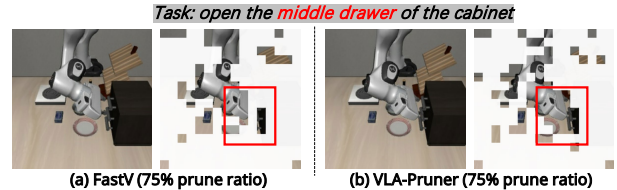


Figure 7. Qualitative case study of VLA-Pruner performance. VLA-Pruner preserves essential localized visual information for precise action execution, while maintaining broad semantic understanding.

only improves short-horizon control but sacrifices semantic grounding and task planning, and thus neither maintains VLA performance well. *Score-fusion* remains inferior to the prefill-only setting. We also ablate the temporal decay window size  $w$  in Fig. 6, which demonstrates the robustness of our method and reveals the short-term temporal continuity of VLA manipulation. When  $w = 1$ , it reduces to using the last timestep’s action attention to guide pruning, leading to performance degradation. We further ablate varying decay rate  $\gamma$  and pruning layer  $K$  in the Appendix B.5.2.

**Qualitative Visualization.** We provide a qualitative case study of VLA-Pruner in Fig. 7. VLA-Pruner preserves essential localized visual information for precise action execution, while maintaining broad semantic understanding.

## 6. Conclusion

We propose VLA-Pruner, a training-free token pruning method for efficient VLA inference. To align with the VLA models’ *dual-system nature* of high-level semantic understanding and low-level action execution, VLA-Pruner employs a dual-level token importance criterion that integrates semantic-level relevance and action-level importance. Based on this criterion, our dual-level token selection strategy adaptively retains visual tokens. Across diverse robotic manipulation tasks and multiple VLA architectures, VLA-Pruner reduces computation while preserving performance. We discuss our limitations in Appendix C.

## References

[1] Harsh Agrawal, Karan Desai, Yufei Wang, Xinlei Chen, Rishabh Jain, Mark Johnson, Dhruv Batra, Devi Parikh, Stefan Lee, and Peter Anderson. Nocaps: Novel object captioning at scale. In *Proceedings of the IEEE/CVF international conference on computer vision*, pages 8948–8957, 2019. 2

[2] Saeed Ranjbar Alvar, Gursimran Singh, Mohammad Akbari, and Yong Zhang. Divprune: Diversity-based visual token pruning for large multimodal models. In *Proceedings of the Computer Vision and Pattern Recognition Conference*, pages 9392–9401, 2025. 1, 2, 3, 5, 6, 4

[3] Jinze Bai, Shuai Bai, Shusheng Yang, Shijie Wang, Sinan Tan, Peng Wang, Junyang Lin, Chang Zhou, and Jingren Zhou. Qwen-vl: A frontier large vision-language model with versatile abilities. *arXiv preprint arXiv:2308.12966*, 1(2):3, 2023. 1

[4] Kevin Black, Noah Brown, Danny Driess, Adnan Esmail, Michael Equi, Chelsea Finn, Niccolò Fusai, Lachy Groom, Karol Hausman, Brian Ichter, et al.  $\pi_0$ : A vision-language-action flow model for general robot control. *arXiv preprint arXiv:2410.24164*, 2024. 1, 2, 3, 6

[5] George EP Box, Gwilym M Jenkins, Gregory C Reinsel, and Greta M Ljung. *Time series analysis: forecasting and control*. John Wiley & Sons, 2015. 5

[6] Peter J Brockwell and Richard A Davis. *Introduction to time series and forecasting*. Springer, 2002. 5

[7] Anthony Brohan, Noah Brown, Justice Carbajal, Yevgen Chebotar, Joseph Dabis, Chelsea Finn, Keerthana Gopalakrishnan, Karol Hausman, Alex Herzog, Jasmine Hsu, et al. Rt-1: Robotics transformer for real-world control at scale. *arXiv preprint arXiv:2212.06817*, 2022. 1, 2, 6

[8] Liang Chen, Haozhe Zhao, Tianyu Liu, Shuai Bai, Junyang Lin, Chang Zhou, and Baobao Chang. An image is worth 1/2 tokens after layer 2: Plug-and-play inference acceleration for large vision-language models. In *European Conference on Computer Vision*, pages 19–35. Springer, 2024. 1, 2, 3, 4, 6

[9] Cheng Chi, Zhenjia Xu, Siyuan Feng, Eric Cousineau, Yilun Du, Benjamin Burchfiel, Russ Tedrake, and Shuran Song. Diffusion policy: Visuomotor policy learning via action diffusion. *The International Journal of Robotics Research*, 44(10-11):1684–1704, 2025. 1

[10] Javier Contreras, Rosario Espinola, Francisco J Nogales, and Antonio J Conejo. Arima models to forecast next-day electricity prices. *IEEE transactions on Power Systems*, 18(3):1114–1121, 2003. 5

[11] Can Cui, Pengxiang Ding, Wenxuan Song, Shuanghao Bai, Xinyang Tong, Zirui Ge, Runze Suo, Wanqi Zhou, Yang Liu, Bofang Jia, et al. Openhelix: A short survey, empirical analysis, and open-source dual-system vla model for robotic manipulation. *arXiv preprint arXiv:2505.03912*, 2025. 2, 3

[12] Tri Dao, Dan Fu, Stefano Ermon, Atri Rudra, and Christopher Ré. Flashattention: Fast and memory-efficient exact attention with io-awareness. *Advances in neural information processing systems*, 35:16344–16359, 2022. 6

[13] Roya Firoozi, Johnathan Tucker, Stephen Tian, Anirudha Majumdar, Jiankai Sun, Weiyu Liu, Yuke Zhu, Shuran Song, Ashish Kapoor, Karol Hausman, et al. Foundation models in robotics: Applications, challenges, and the future. *The International Journal of Robotics Research*, 44(5):701–739, 2025. 1, 3

[14] Everette S. Gardner. Exponential smoothing: The state of the art. *Journal of Forecasting*, 4(1):1–28, 1985. 2, 4, 5

[15] Everette S Gardner Jr. Exponential smoothing: The state of the art—part ii. *International journal of forecasting*, 22(4):637–666, 2006. 2, 5

[16] Suyu Ge, Yunan Zhang, Liyuan Liu, Minjia Zhang, Jiawei Han, and Jianfeng Gao. Model tells you what to discard: Adaptive kv cache compression for llms. *arXiv preprint arXiv:2310.01801*, 2023. 4

[17] M Guha and SK Nandi. Application of arima model for forecasting of daily maximum temperature. *MAUSAM*, 69(2):291–296, 2018. 5

[18] ByungOk Han, Jaehong Kim, and Jinhyeok Jang. A dual process vla: Efficient robotic manipulation leveraging vlm. *arXiv preprint arXiv:2410.15549*, 2024. 2, 3

[19] Chi-Pin Huang, Yueh-Hua Wu, Min-Hung Chen, Yu-Chiang Frank Wang, and Fu-En Yang. Thinkact: Vision-language-action reasoning via reinforced visual latent planning. *arXiv preprint arXiv:2507.16815*, 2025. 2, 3

[20] Drew A Hudson and Christopher D Manning. Gqa: A new dataset for real-world visual reasoning and compositional question answering. In *Proceedings of the IEEE/CVF conference on computer vision and pattern recognition*, pages 6700–6709, 2019. 2

[21] Rob J Hyndman and George Athanasopoulos. *Forecasting: principles and practice*. OTexts, 2018. 4, 5

[22] Moo Jin Kim, Karl Pertsch, Siddharth Karamcheti, Ted Xiao, Ashwin Balakrishna, Suraj Nair, Rafael Rafailov, Ethan Foster, Grace Lam, Pannag Sanketi, et al. Openvla: An open-source vision-language-action model. *arXiv preprint arXiv:2406.09246*, 2024. 1, 2, 3, 6

[23] Moo Jin Kim, Chelsea Finn, and Percy Liang. Fine-tuning vision-language-action models: Optimizing speed and success. *arXiv preprint arXiv:2502.19645*, 2025. 1

[24] Moo Jin Kim, Chelsea Finn, and Percy Liang. Fine-tuning vision-language-action models: Optimizing speed and success. *arXiv preprint arXiv:2502.19645*, 2025. 2, 6, 1

[25] Qixiu Li, Yaobo Liang, Zeyu Wang, Lin Luo, Xi Chen, Mozheng Liao, Fangyun Wei, Yu Deng, Sicheng Xu, Yizhong Zhang, et al. Cogact: A foundational vision-language-action model for synergizing cognition and action in robotic manipulation. *arXiv preprint arXiv:2411.19650*, 2024. 1

[26] Xinghang Li, Minghuan Liu, Hanbo Zhang, Cunjun Yu, Jie Xu, Hongtao Wu, Chilam Cheang, Ya Jing, Weinan Zhang, Huaping Liu, et al. Vision-language foundation models as effective robot imitators. *arXiv preprint arXiv:2311.01378*, 2023. 2

[27] Xuanlin Li, Kyle Hsu, Jiayuan Gu, Karl Pertsch, Oier Mees, Homer Rich Walke, Chuyuan Fu, Ishikaa Lunawat, Isabel Sieh, Sean Kirmani, Sergey Levine, Jiajun Wu, Chelsea Finn, Hao Su, Quan Vuong, and Ted Xiao. Evaluating real-world robot manipulation policies in simulation. *arXiv preprint arXiv:2405.05941*, 2024. 2, 6, 7, 3

[28] Yuncheng Li, Yale Song, Liangliang Cao, Joel Tetreault, Larry Goldberg, Alejandro Jaimes, and Jiebo Luo. Tgif: A new dataset and benchmark on animated gif description. In *Proceedings of the IEEE Conference on Computer Vision and Pattern Recognition*, pages 4641–4650, 2016. 2

[29] Ye Li, Yuan Meng, Zewen Sun, Kangye Ji, Chen Tang, Jiajun Fan, Xinzhong Ma, Shutao Xia, Zhi Wang, and Wenwu Zhu. Sp-vla: A joint model scheduling and token pruning approach for vla model acceleration. *arXiv preprint arXiv:2506.12723*, 2025. 3

[30] Tao Lin, Yilei Zhong, Yuxin Du, Jingjing Zhang, Jiting Liu, Yinxinyu Chen, Encheng Gu, Ziyan Liu, Hongyi Cai, Yanwen Zou, Lixing Zou, Zhaoye Zhou, Gen Li, and Bo Zhao. Evo-1: Lightweight vision-language-action model with preserved semantic alignment, 2025. 1

[31] Zhihang Lin, Mingbao Lin, Luxi Lin, and Rongrong Ji. Boosting multimodal large language models with visual tokens withdrawal for rapid inference. In *Proceedings of the AAAI Conference on Artificial Intelligence*, pages 5334–5342, 2025. 2, 4

[32] Bo Liu, Yifeng Zhu, Chongkai Gao, Yihao Feng, Qiang Liu, Yuke Zhu, and Peter Stone. Libero: Benchmarking knowledge transfer for lifelong robot learning. *Advances in Neural Information Processing Systems*, 36:44776–44791, 2023. 1, 2, 3, 6

[33] Haotian Liu, Chunyuan Li, Qingyang Wu, and Yong Jae Lee. Visual instruction tuning. *Advances in neural information processing systems*, 36:34892–34916, 2023. 1

[34] Yuan Liu, Haodong Duan, Yuanhan Zhang, Bo Li, Songyang Zhang, Wangbo Zhao, Yike Yuan, Jiaqi Wang, Conghui He, Ziwei Liu, et al. Mmbench: Is your multi-modal model an all-around player? In *European conference on computer vision*, pages 216–233. Springer, 2024. 2

[35] Yue Ma, Zixing Song, Yuzheng Zhuang, Jianye Hao, and Irwin King. A survey on vision-language-action models for embodied ai. *arXiv preprint arXiv:2405.14093*, 2024. 1

[36] Junzhu Mao, Yang Shen, Jinyang Guo, Yazhou Yao, and Xianzheng Hua. Efficient token compression for vision transformer with spatial information preserved. *arXiv preprint arXiv:2503.23455*, 2025. 2

[37] Junzhu Mao, Yang Shen, Jinyang Guo, Yazhou Yao, Xianzheng Hua, and Hengtao Shen. Prune and merge: Efficient token compression for vision transformer with spatial information preserved. *IEEE Transactions on Multimedia*, 2025. 2

[38] Rafael Martí, Anna Martínez-Gavara, Sergio Pérez-Peló, and Jesús Sánchez-Oro. A review on discrete diversity and dispersion maximization from an or perspective. *European Journal of Operational Research*, 299(3):795–813, 2022. 6

[39] Naufel B Mhammed, Soran Ab M Saeed, and Avan M Ahmed. Eog signal modeling using double exponential smoothing for robot arm control system. *Kurdistan Journal of Applied Research*, 1(3):6–10, 2016. 5

[40] Abby O’Neill, Abdul Rehman, Abhiram Maddukuri, Abhishek Gupta, Abhishek Padalkar, Abraham Lee, Acorn Polley, Agrim Gupta, Ajay Mandlekar, Ajinkya Jain, et al. Open x-embodiment: Robotic learning datasets and rt-x models: Open x-embodiment collaboration 0. In *2024 IEEE International Conference on Robotics and Automation (ICRA)*, pages 6892–6903. IEEE, 2024. 1, 2

[41] Seongmin Park, Hyungmin Kim, Wonseok Jeon, Juyoung Yang, Byeongwook Jeon, Yoonseon Oh, and Jungwook Choi. Quantization-aware imitation-learning for resource-efficient robotic control. *arXiv preprint arXiv:2412.01034*, 2024. 1

[42] Hanchuan Peng, Fuhui Long, and Chris Ding. Feature selection based on mutual information criteria of max-dependency, max-relevance, and min-redundancy. *IEEE Transactions on pattern analysis and machine intelligence*, 27(8):1226–1238, 2005. 2, 5

[43] M Hashem Pesaran and Ron P Smith. Empirical macroeconomic modelling for policy analysis. *The Oxford Handbook of Economic Forecasting*, 2012. 5

[44] Bryan A Plummer, Liwei Wang, Chris M Cervantes, Juan C Caicedo, Julia Hockenmaier, and Svetlana Lazebnik. Flickr30k entities: Collecting region-to-phrase correspondences for richer image-to-sentence models. In *Proceedings of the IEEE international conference on computer vision*, pages 2641–2649, 2015. 2

[45] Daniel Cosmin Porumbel, Jin-Kao Hao, and Fred Glover. A simple and effective algorithm for the maxmin diversity problem. *Annals of Operations Research*, 186(1):275–293, 2011. 6

[46] Mauricio GC Resende, Rafael Martí, Micael Gallego, and Abraham Duarte. Grasp and path relinking for the max-min diversity problem. *Computers & Operations Research*, 37(3):498–508, 2010. 6

[47] Yuzhang Shang, Mu Cai, Bingxin Xu, Yong Jae Lee, and Yan Yan. Llava-prumerge: Adaptive token reduction for efficient large multimodal models. *arXiv preprint arXiv:2403.15388*, 2024. 1, 2

[48] Steven A Sloman. The empirical case for two systems of reasoning. *Psychological bulletin*, 119(1):3, 1996. 2, 3

[49] Hugo Touvron, Louis Martin, Kevin Stone, Peter Albert, Amjad Almahairi, Yasmine Babaei, Nikolay Bashlykov, Soumya Batra, Prajwal Bhargava, Shruti Bhosale, et al. Llama 2: Open foundation and fine-tuned chat models. *arXiv preprint arXiv:2307.09288*, 2023. 2

[50] Hanzhen Wang, Jiaming Xu, Jiayi Pan, Yongkang Zhou, and Guohao Dai. Specprune-vla: Accelerating vision-language-action models via action-aware self-speculative pruning. *arXiv preprint arXiv:2509.05614*, 2025. 3

[51] Junjie Wen, Yichen Zhu, Jinming Li, Minjie Zhu, Zhibin Tang, Kun Wu, Zhiyuan Xu, Ning Liu, Ran Cheng, Chaomin Shen, et al. Tinyvla: Towards fast, data-efficient vision-language-action models for robotic manipulation. *IEEE Robotics and Automation Letters*, 2025. 1

[52] Peter R Winters. Forecasting seasonals and trends by exponentially weighted moving averages. *Management science*, 6(3):324–342, 1960. 4, 5

[53] Long Xing, Qidong Huang, Xiaoyi Dong, Jiajie Lu, Pan Zhang, Yuhang Zang, Yuhang Cao, Conghui He, Jiaqi Wang, Feng Wu, et al. Pyramiddrop: Accelerating your large vision-language models via pyramid visual redundancy reduction. *arXiv preprint arXiv:2410.17247*, 2024. 1

[54] Dejing Xu, Zhou Zhao, Jun Xiao, Fei Wu, Hanwang Zhang, Xiangnan He, and Yueling Zhuang. Video question answering via gradually refined attention over appearance and motion. In *Proceedings of the 25th ACM international conference on Multimedia*, pages 1645–1653, 2017. 2

[55] Siyu Xu, Yunke Wang, Chenghao Xia, Dihao Zhu, Tao Huang, and Chang Xu. Vla-cache: Efficient vision-language-action manipulation via adaptive token caching. In *The Thirty-ninth Annual Conference on Neural Information Processing Systems*. 2, 3, 4, 5, 6

[56] Yantai Yang, Yuhao Wang, Zichen Wen, Luo Zhongwei, Chang Zou, Zhipeng Zhang, Chuan Wen, and Linfeng Zhang. EfficientVLA: Training-free acceleration and compression for vision-language-action models. In *The Thirty-ninth Annual Conference on Neural Information Processing Systems*, 2025. 3, 6, 4

[57] Weihao Ye, Qiong Wu, Wenhao Lin, and Yiyi Zhou. Fit and prune: Fast and training-free visual token pruning for multi-modal large language models. In *Proceedings of the AAAI Conference on Artificial Intelligence*, pages 22128–22136, 2025. 1, 2, 4

[58] Zhaoshu Yu, Bo Wang, Pengpeng Zeng, Haonan Zhang, Ji Zhang, Lianli Gao, Jingkuan Song, Nicu Sebe, and Heng Tao Shen. A survey on efficient vision-language-action models, 2025. 3

[59] Yang Yue, Yulin Wang, Bingyi Kang, Yizeng Han, Shenzhi Wang, Shiji Song, Jiashi Feng, and Gao Huang. Deer-vla: Dynamic inference of multimodal large language models for efficient robot execution. *Advances in Neural Information Processing Systems*, 37:56619–56643, 2024. 1

[60] Yuan Zhang, Chun-Kai Fan, Junpeng Ma, Wenzhao Zheng, Tao Huang, Kuan Cheng, Denis Gudovskiy, Tomoyuki Okuno, Yohei Nakata, Kurt Keutzer, et al. Sparsevlm: Visual token sparsification for efficient vision-language model inference. *arXiv preprint arXiv:2410.04417*, 2024. 1, 2, 3, 4, 6

[61] Zhenyu Zhang, Ying Sheng, Tianyi Zhou, Tianlong Chen, Lianmin Zheng, Ruiqi Cai, Zhao Song, Yuandong Tian, Christopher Ré, Clark Barrett, et al. H2o: Heavy-hitter oracle for efficient generative inference of large language models. *Advances in Neural Information Processing Systems*, 36: 34661–34710, 2023. 4

[62] Qingqing Zhao, Yao Lu, Moo Jin Kim, Zipeng Fu, Zhuoyang Zhang, Yecheng Wu, Zhaoshuo Li, Qianli Ma, Song Han, Chelsea Finn, et al. Cot-vla: Visual chain-of-thought reasoning for vision-language-action models. In *Proceedings of the Computer Vision and Pattern Recognition Conference*, pages 1702–1713, 2025. 1

[63] Brianna Zitkovich, Tianhe Yu, Sichun Xu, Peng Xu, Ted Xiao, Fei Xia, Jialin Wu, Paul Wohlhart, Stefan Welker, Ayzaan Wahid, et al. Rt-2: Vision-language-action models transfer web knowledge to robotic control. In *Conference on Robot Learning*, pages 2165–2183. PMLR, 2023. 1, 2, 6

[64] Xin Zou, Di Lu, Yizhou Wang, Yibo Yan, Yuanhuiyi Lyu, Xu Zheng, Linfeng Zhang, and Xuming Hu. Don't just chase “highlighted tokens” in mllms: Revisiting visual holistic context retention. In *The Thirty-ninth Annual Conference on Neural Information Processing Systems*. 1, 2, 4

# VLA-Pruner: Temporal-Aware Dual-Level Visual Token Pruning for Efficient Vision-Language-Action Inference

## Supplementary Material

### A. Method Details

#### A.1. Algorithm Outlines

We detail VLA-Pruner in Algorithm 1 (min-redundancy filtering) and Algorithm 2 (overall dual-level token selection).

#### A.2. Complexity Analysis

Following FastV [8], SparseVLM [60] and DivPrune [2], we estimate the computational requirement of VLA-Pruner in terms of Transformer FLOPs, and focus on how pruning visual tokens changes the effective sequence length seen by each layer. As in prior work [2], we count the FLOPs of multi-head attention and feed-forward networks (FFNs) in the backbone (the overhead of token selection as negligible compared to the main model FLOPs.) Let  $T$  be the total number of Transformer layers in the VLA backbone and  $K$  the index of the pruning layer. Denote the numbers of text and visual tokens before pruning by  $N$  and  $M$  ( $M \gg N$ ), and let  $\mu = N + M$  be the full sequence length. After VLA-Pruner keeps a fraction  $\rho$  of the visual tokens, the sequence length becomes  $\tilde{\mu} = N + \rho M$ . Following [8], the FLOPs of attention and FFN for one layer with sequence length  $n$ , hidden size  $d$ , and FFN intermediate size  $m$  can be approximated as

$$C(n) = 4nd^2 + 2n^2d + 2ndm. \quad (10)$$

Without pruning, the total FLOPs are

$$\text{FLOPs}_{\text{full}} = T C(\mu). \quad (11)$$

With VLA-Pruner, the first  $K$  layers still use the full sequence  $\mu$ , while the remaining  $T - K$  layers use the shortened sequence  $\tilde{\mu}$ , giving

$$\text{FLOPs}_{\text{prune}} = K C(\mu) + (T - K) C(\tilde{\mu}). \quad (12)$$

Thus, the theoretical FLOPs ratio is

$$r_{\text{FLOPs}} = \frac{\text{FLOPs}_{\text{prune}}}{\text{FLOPs}_{\text{full}}} = \frac{KC(\mu) + (T - K)C(\tilde{\mu})}{TC(\mu)}. \quad (13)$$

Since the attention term in  $C(\cdot)$  is quadratic in sequence length, the reduction scales roughly with  $\rho^2$  in layers after  $K$ . This matches the empirical FLOPs ratios in Tab. 1: VLA-Pruner reduces FLOPs to about 60%, 40%, and 30% of the original model at 50%, 25%, and 12.5% token retention, respectively. Temporal smoothing over a short window of action-to-vision attention has complexity  $O(wM)$

per timestep, and the greedy Max-Min filtering over the dual-level candidate pool of size  $O(\rho M)$  is  $O((\rho M)^2)$  per prefill. In practice, these components contribute little to the total wall-clock time, as these operations are invoked only once during the prefill stage. Finally, Eq. (13) shows that VLA-Pruner offers a flexible way to trade accuracy for efficiency: the retained-token ratio  $\rho \in (0, 1]$ . Smaller  $\rho$  reduces FLOPs quadratically in layers after  $K$ , yielding higher speedup, while larger  $\rho$  recovers the original model’s performance. In our experiments, we report results at  $\rho \in 0.5, 0.25, 0.125$ , but VLA-Pruner can be used at any intermediate ratio to meet a given compute or latency target.

### B. Experiments Details

#### B.1. Setting up Details

##### B.1.1. VLA Model Details

We consider three representative VLA architectures in our experiments: OpenVLA, OpenVLA-OFT, and  $\pi_0$ . All models take RGB observations and a natural language instruction as input, and produce robot actions end-to-end.

**OpenVLA.** OpenVLA [22] is a 7B-parameter open-source vision-language-action model built by fine-tuning a Prismatic VLM (Llama 2 language backbone with DINOv2 and SigLIP visual encoders) on robot manipulation episodes from the Open X-Embodiment dataset. The model represents actions as discrete tokens and decodes them autoregressively, enabling a single policy to control multiple embodiments out-of-the-box. OpenVLA serves as our base autoregressive VLA, and we follow its official checkpoints and evaluation settings on LIBERO.

**OpenVLA-OFT.** OpenVLA-OFT [24] is an “Optimized Fine-Tuning” variant of OpenVLA that improves both control performance and inference efficiency. It augments the original decoder with parallel decoding and action chunking, and switches to a continuous action representation trained with a simple L1 regression objective. This substantially boosts success rates on LIBERO while increasing action-generation throughput. To be noted, OpenVLA-OFT utilizes bidirectional attention, meaning that during inference, there is already an action-to-vision cross-attention. However, we observe that during the early-layer prefill phase, the attention still focuses on semantic understanding, making action-to-vision less significant. In deeper layers, the action-to-vision attention starts to exhibit more distinct properties. This allows our method to effectively enhance token pruning performance by utilizing past timestep

---

**Algorithm 1** Redundancy-Minimization Filtering

---

**Require:** Visual embeddings  $\mathbf{E}_v = \{v_1, \dots, v_M\}$ , candidate index set  $\mathcal{C}_{\text{dual}} \subseteq \{1, \dots, M\}$ , target size  $\tilde{M}$   
**Ensure:** Selected index set  $\tilde{\mathcal{C}}$ , with  $|\tilde{\mathcal{C}}| = \tilde{M}$

```

1: if  $|\mathcal{C}_{\text{dual}}| \leq \tilde{M}$  then
2:   return  $\mathcal{C}_{\text{dual}}$ 
3: end if
4: Extract candidate features:  $\{v_i\}_{i \in \mathcal{C}_{\text{dual}}}$ 
5: Normalize:  $u_i \leftarrow v_i / \|v_i\|_2$  for all  $i \in \mathcal{C}_{\text{dual}}$ 
6: Compute cosine distance matrix  $D$  over  $\mathcal{C}_{\text{dual}}$ :  $D_{ij} \leftarrow 1 - u_i^\top u_j$ 
7:  $\tilde{\mathcal{C}} \leftarrow \emptyset$  ▷ Initialize by maximal second-nearest distance
8: for each  $i \in \mathcal{C}_{\text{dual}}$  do
9:   Let  $\{d_{i1}, d_{i2}, \dots\}$  be  $D_{ij}$  for  $j \in \mathcal{C}_{\text{dual}}, j \neq i$  sorted increasingly
10:   $s_i \leftarrow d_{i2}$  ▷ second smallest distance
11: end for
12:  $i^* \leftarrow \arg \max_{i \in \mathcal{C}_{\text{dual}}} s_i$ 
13:  $\tilde{\mathcal{C}} \leftarrow \tilde{\mathcal{C}} \cup \{i^*\}$ 
14: while  $|\tilde{\mathcal{C}}| < \tilde{M}$  do
15:   for each  $j \in \mathcal{C}_{\text{dual}} \setminus \tilde{\mathcal{C}}$  do
16:      $m_j \leftarrow \min_{i \in \tilde{\mathcal{C}}} D_{ij}$  ▷ min distance to selected set
17:   end for
18:    $j^* \leftarrow \arg \max_{j \in \mathcal{C}_{\text{dual}} \setminus \tilde{\mathcal{C}}} m_j$ 
19:    $\tilde{\mathcal{C}} \leftarrow \tilde{\mathcal{C}} \cup \{j^*\}$ 
20: end while
21: return  $\tilde{\mathcal{C}}$ 

```

---

**Algorithm 2** Dual-Level Token Selection (Combine-then-Filter)

---

**Require:** Visual embeddings  $\mathbf{E}_v = \{v_1, \dots, v_M\}$ ; Semantic scores  $\mathcal{S}_{\text{vl}} \in \mathbb{R}^M$ ; Action scores  $\hat{\mathcal{S}}_{\text{act}} \in \mathbb{R}^M$ ; Token budget  $\tilde{M}$   
**Ensure:** Selected index set  $\tilde{\mathcal{C}} \subseteq \{1, \dots, M\}$ , with  $|\tilde{\mathcal{C}}| = \tilde{M}$

```

1: if  $\tilde{M} \geq M$  then
2:   return  $\{1, \dots, M\}$  ▷ no pruning
3: end if
4:  $\mathcal{C}_{\text{vl}} \leftarrow$  indices of Top- $\tilde{M}$  elements of  $\mathcal{S}_{\text{vl}}$ 
5:  $\mathcal{C}_{\text{act}} \leftarrow$  indices of Top- $\tilde{M}$  elements of  $\hat{\mathcal{S}}_{\text{act}}$ 
6: Max-Relevance pooling:  $\mathcal{C}_{\text{dual}} \leftarrow \mathcal{C}_{\text{vl}} \cup \mathcal{C}_{\text{act}}$ 
7: Min-Redundancy filtering:  $\tilde{\mathcal{C}} \leftarrow \text{REDUNDANCY-MINIMIZATION FILTERING}(\mathbf{E}_v, \mathcal{C}_{\text{dual}}, \tilde{M})$  ▷ Alg. 1
8: return  $\tilde{\mathcal{C}}$ 

```

---

action-to-vision cross-attention at the later layers to guide current token pruning.

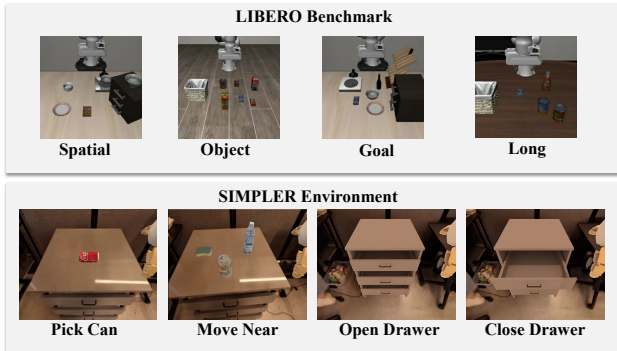
$\pi_0$  **Model.**  $\pi_0$  [4] is a prototype generalist robot policy that augments a pretrained vision-language model (with a PaliGemma backbone) with a continuous-action flow-matching head. Built on top of a large VLM to inherit Internet-scale semantic knowledge,  $\pi_0$  is trained on diverse real-robot data and is designed for high-frequency control in dexterous manipulation tasks. The model decodes continuous motor commands via a flow-matching process with 10 integration steps. We use  $\pi_0$  as a diffusion-based VLA backbone to evaluate the generality of VLA-Pruner. To capture the most informative action-to-vision interactions, we record the action-to-vision cross-attention averaged over the latter half of these integration steps, where the cross-attention becomes more stable and reliable.

### B.1.2. Acceleration Baseline Details

We briefly summarize the baseline acceleration methods considered in our experiments.

**FastV.** FastV [8](ECCV24) accelerates large vision-language models by pruning redundant visual tokens based on early-layer prefill attention. Its core observation is that many image patches receive consistently low attention in deeper layers while contributing substantially to computation. FastV defines an attention-based importance score during the prefill stage and drops a fixed fraction of low-score visual tokens after a chosen layer. It is training-free and purely semantic, but does not account for the action-dependent requirements of VLA models.

**SparseVLM.** SparseVLM [60](ICML25) also targets visual token redundancy in VLMs, but uses text-to-vision cross-attention as the importance signal. Tokens that receive



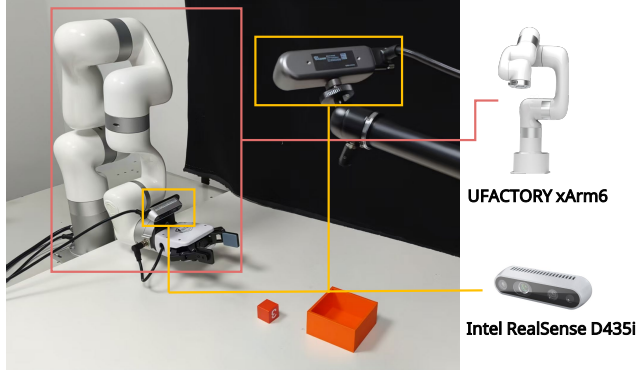
(a) Tasks on LIBERO benchmark and the SIMPLER environment.

low cross-attention from text queries are considered less relevant and pruned. Compared to FastV, SparseVLM focuses directly on aligning visual tokens with language semantics, yet still operates only at the semantic level and ignores the distinct visual needs of action decoding in VLA.

**DivPrune.** DivPrune [2](CVPR25) addresses the tendency of attention-based methods to select similar and redundant tokens. Instead of ranking tokens by attention scores, it formulates token selection as a Max–Min Diversity Problem and chooses a subset of visual tokens that are maximally dissimilar in feature space, thereby reducing redundancy while maintaining coverage. However, DivPrune is agnostic to the dual-level relevance of visual tokens in VLA prefilling and action decoding, and its diversity objective fall short for VLA tasks where localized details are more critical.

**VLA-Cache.** VLA-Cache [55](Neurips25) is a training-free acceleration method tailored for VLA models. It exploits temporal continuity in robotic manipulation by identifying visually static tokens whose features change little across timesteps, and reuses their computation via a KV-cache. At the same time, it uses text-to-vision cross-attention to keep task-relevant tokens fully computed. This cache-based mechanism reduces repeated computation over static background regions, but its token selection remains coarse-grained, which does not explicitly consider action-to-vision attention as we do. To ensure a fair comparison, we set the dynamic token limit based on similarity to be  $1.5 \times k$  ( $k$  is the token budget), and use text-to-vision score to exclude  $0.5 \times k$  of the most relevant tokens. These settings follow the default setup of VLA-Cache codebase.

**EfficientVLA.** EfficientVLA [56](Neurips25) proposes a structured acceleration framework for VLA models that combines visual token pruning, layer reduction, and diffusion temporal feature caching. Its token-pruning component leverages attention and diversity heuristics inherited from VLM pruning, while additional modules (i.e., layer skipping and diffusion caching) are used to achieve comparable acceleration. In contrast, VLA-Pruner is a single, plug-and-play token pruning module. These



(b) Real-world xArm6 robot setup.

approaches are therefore complementary: EfficientVLA and other VLA acceleration methods can be adopted orthogonally with VLA-Pruner, while VLA-Pruner achieves strongest token-prune performance.

## B.2. Benchmark Details

Fig. 8a shows the evaluation simulation environments and Fig. 8b presents our real-world xArm6 robot setup.

**LIBERO.** LIBERO [32] is a Robosuite-based benchmark for lifelong robot manipulation that groups 130 language-conditioned tasks into four suites: *Spatial*, *Object*, *Goal*, and *Long*. LIBERO-Spatial varies only the spatial configuration of otherwise identical objects (e.g., pick up the black bowl on the stove and place it on the plate). LIBERO-Object varies the manipulated object while keeping the scene layout and goal template fixed (e.g., pick up the bbq sauce and place it in the basket). LIBERO-Goal keeps both the objects and spatial layout fixed but changes the goal description (e.g., open the middle drawer of the cabinet). LIBERO-Long corresponds to the long-horizon subset (10 tasks) of LIBERO-100, where each episode consists of multi-stage instructions such as opening a drawer, inserting an object, and then rearranging other items(e.g., put both the alphabet soup and the cream cheese box in the basket).

**SIMPLER.** SIMPLER [27] is a simulation suite built to closely track the real Google robot environment while allowing controlled appearance variation. It provides two evaluation settings. The *Visual Matching* (VM) setting keeps backgrounds, lighting, distractors, and camera poses close to the real setup so that rendered observations visually resemble real robot scenes and better predict real-world performance. The *Variant Aggregation* (VA) setting starts from the same base scenes but procedurally perturbs nuisance factors such as background textures, illumination, number and placement of distractor objects, table material, and camera viewpoints, creating a broad distribution shift for testing robustness. For the Google robot configuration, SIMPLER defines four canonical manipulation tasks: “pick coke can”, “pick object”, “move near”, “open/close

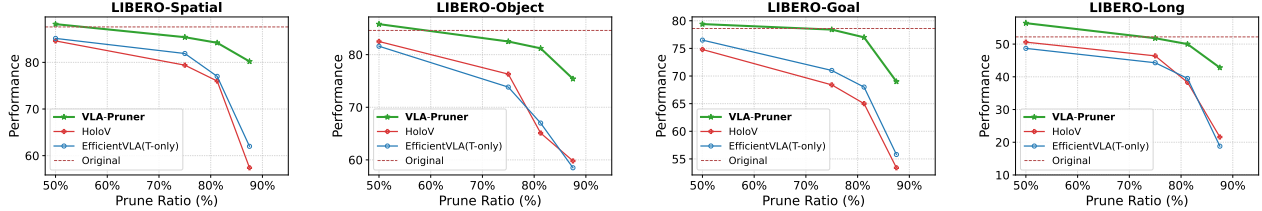


Figure 9. Performance of OpenVLA with more baseline methods across LIBERO tasks under varying prune ratio. The horizontal axis represents the pruning/caching ratios of visual tokens, and the vertical axis shows the success rates.

Table 3. Performance comparison with various pruning methods.

| Method                   | Spatial | Object | Goal | Long | Avg. $\uparrow$ | FLOPs $\downarrow$ | Speedup $\uparrow$ |
|--------------------------|---------|--------|------|------|-----------------|--------------------|--------------------|
| VLA-Pruner               | 85.4    | 82.5   | 78.4 | 51.8 | 74.5            | 39.80%             | 1.633 $\times$     |
| EfficientVLA (w/o layer) | 85.1    | 81.6   | 76.5 | 51.7 | 73.7            | 58.12%             | 1.334 $\times$     |
| EfficientVLA             | 84.9    | 80.3   | 76.1 | 50.3 | 72.9            | 41.30%             | 1.491 $\times$     |
| VTW                      | 74.7    | 76.2   | 72.3 | 48.9 | 68.0            | 55.17%             | 1.325 $\times$     |
| FitPrune                 | 82.4    | 80.1   | 74.8 | 50.3 | 71.9            | 47.71%             | 1.397 $\times$     |

Drawer”, and “place in closed drawer”. In our experiments, we follow the official simulator settings and success metrics, and report results on three representative tasks—*Pick Coke Can*, *Move Near*, and *Open/Close Drawer*—under VM or VA setting.

**Real robot.** As shown in Figure 8b, our real-world system is built on a 6-DoF xArm6 manipulator equipped with two Intel RealSense D435i RGB cameras: one mounted on the wrist for close-range observations and the other fixed for capturing global scene context. The robot is controlled through the official xArmAPI. We collect real-world demonstrations following the LeRobot 2.1 data specification. Each episode consists of synchronized observations recorded at 30Hz, including two RGB image streams. The proprioceptive state is represented by the robot’s absolute joint angles, and actions are stored using the same absolute joint angles to ensure consistent replay and supervision. All demonstrations are gathered using this unified multi-view setup, which provides both global scene context and fine-grained manipulation details that are essential for learning robust visuomotor policies.

### B.3. Results of More Baselines

**Varying pruning ratio.** Besides the main training-free baselines in the paper (FastV [8], SparseVLM [60], Di-vPrune [2], VLA-Cache [55]), we evaluate two recent visual token pruning methods with controllable pruning ratios:token-pruning module from EfficientVLA [56] and the HoloV(Neurips25) pruner [64]. We evaluate them on OpenVLA backbone across four LIBERO suites. For each method, we report the average success rates under varying retained token ratios in Fig. 9. VLA-Pruner achieves consistent superiority across all suites. These results further support that semantic-only token pruning is fragile for VLA, and that a dual-level, redundancy-aware strategy better matches the requirements of embodied control.

**Comparison under comparable performance.** We compare VLA-Pruner against structured and calibration-based baselines, focusing on the trade-off between VLA performance and computational cost. We consider the full EfficientVLA framework [56], which combines token pruning and layer reduction, as well as the calibration-based methods FitPrune [57] and VTW [31]. For EfficientVLA, we set the visual-token retention at 50% and reduce 8 layers to ensure comparable performance while maximizing acceleration. We report VLA-Pruner at 25% token retention, which achieves the better performance while requiring fewer FLOPs and lower latency. This suggests that dual-level VLA token pruning can achieve a better efficiency–performance trade-off than EfficientVLA, which is designed primarily for diffusion head policy and overlook the intrinsic characteristics of VLA inference for token pruning, thereby showing limited performance. For FitPrune and VTW, we follow their official calibration protocols and perform calibration on 100 LIBERO tasks, which corresponds to a substantially larger calibration fraction than that typically used in VLM benchmarks. Both methods achieve lower success rates than VLA-Pruner at 25% token retention and consume more FLOPs (Tab. 3). VTW typically chooses a late withdrawal layer and degrades VLA performance, while FitPrune, though effective on standard VLM benchmarks, shows limited favorable trade-off in the VLA setting since it stills rely on semantic attention scores.

### B.4. Results of $\pi_0$ on LIBERO

**Setup.** We evaluate VLA-Pruner on the  $\pi_0$  model across LIBERO benchmark at various token retention ratios (50%, 25%, and 12.5%). For each configuration, we measure success rates, relative accuracy, latency, speedup, and FLOP ratios. We set the number of flow matching integration steps as 10, action chunk as 50 and execute 5 actions per step.

**Main Results.** VLA-Pruner consistently achieves high per-

Table 4. **Performance of VLA-Pruner on  $\pi_0$  across LIBERO** at different vision-token retention ratios. We report success rates (%) on the four suites, average relative accuracy w.r.t. the vanilla model, latency (ms), speedup and FLOP ratio (%).

| Method                     | LIBERO Success (%) |              |              |              | Avg. (%)      | Acc. (%) $\uparrow$ | Latency(ms) $\downarrow$ | Speedup ( $\times$ ) $\uparrow$ | FLOP ratio (%) |
|----------------------------|--------------------|--------------|--------------|--------------|---------------|---------------------|--------------------------|---------------------------------|----------------|
|                            | Spatial            | Object       | Goal         | Long         |               |                     |                          |                                 |                |
| <i>Upper Bound (100%)</i>  |                    |              |              |              |               |                     |                          |                                 |                |
| Vanilla                    | 96.9               | 98.3         | 96.1         | 84.8         | 94.025        | 100.0               | 104.53                   | 1.000                           | 100            |
| <i>Retain 50% Tokens</i>   |                    |              |              |              |               |                     |                          |                                 |                |
| FastV                      | 95.26              | 95.46        | 92.58        | 81.34        | 91.16         | 96.92               | 66.44                    | 1.573                           | 60.7           |
| SparseVLM                  | 94.70              | 93.96        | 91.50        | 79.48        | 89.91         | 95.48               | 70.39                    | 1.485                           | 61.5           |
| DivPrune                   | 91.30              | 92.14        | 88.25        | 77.19        | 87.22         | 92.61               | 69.17                    | 1.511                           | 58.9           |
| VLA-Cache                  | 96.47              | 95.99        | 96.59        | 84.65        | 93.43         | 99.54               | 78.30                    | 1.335                           | 72.3           |
| <b>VLA-Pruner</b>          | <b>97.01</b>       | <b>98.61</b> | <b>97.57</b> | <b>87.12</b> | <b>100.89</b> | <b>100.11</b>       | <b>69.45</b>             | <b>1.505</b>                    | <b>60.9</b>    |
| <i>Retain 25% Tokens</i>   |                    |              |              |              |               |                     |                          |                                 |                |
| FastV                      | 88.28              | 78.81        | 86.38        | 73.61        | 81.77         | 86.97               | 57.68                    | 1.812                           | 39.9           |
| SparseVLM                  | 89.63              | 84.78        | 81.80        | 72.67        | 82.22         | 86.76               | 61.09                    | 1.711                           | 41.3           |
| DivPrune                   | 84.41              | 71.60        | 80.61        | 66.60        | 75.80         | 80.76               | 59.05                    | 1.770                           | 39.3           |
| VLA-Cache                  | 85.60              | 85.32        | 85.94        | 73.97        | 82.71         | 87.86               | 64.81                    | 1.613                           | 51.4           |
| <b>VLA-Pruner</b>          | <b>95.28</b>       | <b>96.25</b> | <b>95.71</b> | <b>84.04</b> | <b>98.78</b>  | <b>98.78</b>        | <b>60.38</b>             | <b>1.731</b>                    | <b>40.1</b>    |
| <i>Retain 12.5% Tokens</i> |                    |              |              |              |               |                     |                          |                                 |                |
| FastV                      | 68.31              | 59.15        | 57.97        | 28.08        | 53.38         | 57.82               | 51.72                    | 2.021                           | 30.1           |
| SparseVLM                  | 72.04              | 64.98        | 63.55        | 30.99        | 57.89         | 60.71               | 53.79                    | 1.943                           | 31.3           |
| DivPrune                   | 63.41              | 63.78        | 62.79        | 29.61        | 54.90         | 57.33               | 52.64                    | 1.986                           | 29.8           |
| VLA-Cache                  | 59.85              | 58.69        | 64.71        | 27.09        | 52.58         | 55.88               | 59.02                    | 1.771                           | 39.4           |
| <b>VLA-Pruner</b>          | <b>89.64</b>       | <b>90.55</b> | <b>86.60</b> | <b>65.56</b> | <b>87.97</b>  | <b>87.97</b>        | <b>53.49</b>             | <b>1.954</b>                    | <b>30.4</b>    |

Table 5. **Memory and Runtime Analysis of Pruning Methods on OpenVLA**. Detailed comparison of maximum GPU memory consumption and CUDA runtime across different vision-token retention rates.

| Method  | 50% Retained                 |                             | 25% Retained                 |                             | 12.5% Retained               |                             |
|---|------------------------------|-----------------------------|------------------------------|-----------------------------|------------------------------|-----------------------------|
|   | Max Memory (GB) $\downarrow$ | CUDA Time (ms) $\downarrow$ | Max Memory (GB) $\downarrow$ | CUDA Time (ms) $\downarrow$ | Max Memory (GB) $\downarrow$ | CUDA Time (ms) $\downarrow$ |
| Origin Memory: 14.75 GB / Origin CUDA Latency: 51.43 ms |                              |                             |                              |                             |                              |                             |
| Vanilla   |                              |                             |                              |                             |                              |                             |
| FastV   | 14.513                       | 29.022                      | 14.327                       | 25.58                       | 14.311                       | 24.33                       |
| SparseVLM   | 14.544                       | 29.594                      | 14.351                       | 25.71                       | 14.329                       | 23.64                       |
| DivPrune  | 14.438                       | 28.052                      | 14.303                       | 24.98                       | 14.281                       | 22.91                       |
| VLA-Cache   | 14.592                       | 36.33                       | 14.523                       | 35.13                       | 14.484                       | 34.57                       |
| <b>VLA-Pruner</b>                                       | <b>14.527</b>                | <b>29.192</b>               | <b>14.348</b>                | <b>25.58</b>                | <b>14.322</b>                | <b>23.35</b>                |

formance across all token retention settings. Notably, at each tested token retention ratio, our method maintains superior performance relative to other baselines, especially as pruning ratio increases. In particular, for  $\pi_0$ , our method demonstrates impressive efficiency, maintaining comparable success rates even at 12.5% token retention. This enables a significant acceleration in computation while preserving performance, a key advantage over traditional pruning methods. While VLA-Pruner’s redundancy filtering slightly affects acceleration performance on  $\pi_0$  with high-frequency, the impact remains minimal. Even at a 25% retention ratio, VLA-Pruner surpasses other token pruning methods at 50% retention ratio, demonstrating that our method can precisely preserve essential information. The results in Table 4 clearly illustrate how VLA-Pruner maintains robust task success across pruning ratios, highlighting its cross-architecture generalizability to provide an superior trade-off between computational efficiency and model accuracy for diffusion-based model.

## B.5. More results

### B.5.1. Detailed Efficiency Results

We report additional efficiency results, including peak GPU memory consumption (GB) and CUDA runtime (ms), across different vision-token retention ratios. As shown in Table 5, VLA-Pruner exhibits comparable efficiency to

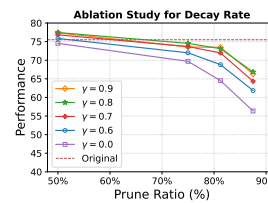


Figure 10. Ablation study for decay rate.

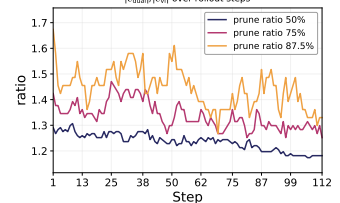


Figure 11.  $|C_{\text{dual}}|/|C_{\text{vl}}|$  ratio trends at different pruning ratios for a task.

| Method     | TFLOP (ratio %) | Spatial | Object | Goal | Long | Avg   |
|------------|-----------------|---------|--------|------|------|-------|
| K=2        | 37.90           | 69.7    | 74.1   | 55.3 | 34.8 | 58.48 |
| K=3 (Ours) | 39.77           | 85.4    | 82.5   | 78.4 | 51.8 | 74.53 |
| K=4        | 41.98           | 85.5    | 82.3   | 78.1 | 52.0 | 74.48 |
| K=5        | 43.08           | 83.9    | 81.7   | 77.9 | 51.4 | 73.73 |

Table 6. Ablation study on applying pruning at different layers.

other pruning methods.

### B.5.2. More ablation studies

**Decay rate  $\gamma$ .** We ablate different decay rates  $\gamma \in \{0.0, 0.6, 0.7, 0.8, 0.9\}$ , and report the results for average success rates under varying prune ratio in Fig. 10.

**Pruning layer  $K$ .** We compare results of different pruning layer values  $K \in \{2, 3, 4, 6\}$  in Table 6.

**VLA-Pruner details.** We show  $|C_{\text{dual}}|/|C_{\text{vl}}|$  ratio trends at different pruning ratios within a robotic task in Fig. 11.

## B.6. More Visualization

We provide detailed visualization of VLA-Pruner token prune results across LIBERO tasks under diverse ratios in Fig. 12. VLA-Pruner maintains both local details for action execution and global information for semantic understanding and task planning.

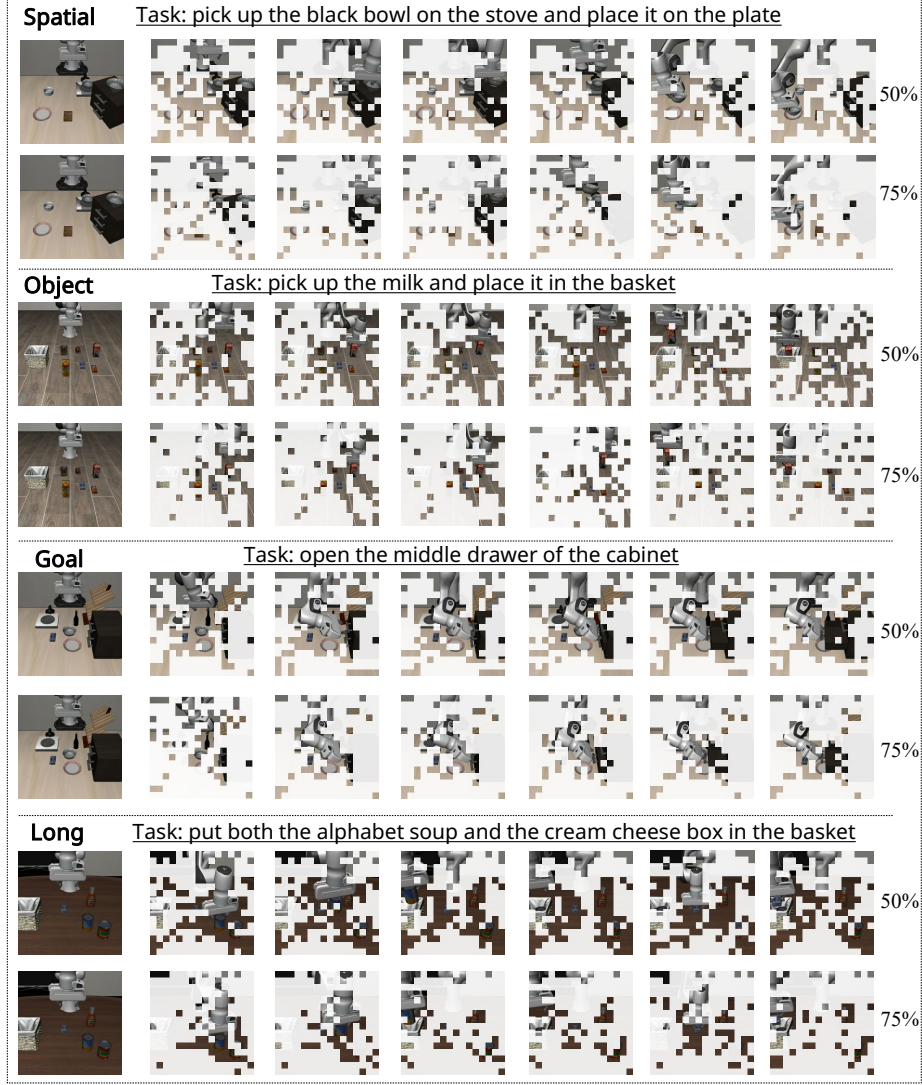


Figure 12. Visualization of VLA-Pruner token pruning results across LIBERO tasks under diverse ratios

## C. Limitations and Future work.

Our main contribution is to point out the dual-system nature of VLA inference and to propose a dual-level importance criterion that jointly accounts for semantic and action-level relevance. However, our current estimation of action-level importance relies on a heuristic temporal smoothing scheme with a fixed window and decay rate. While this works well for most tabletop settings, its benefits may diminish in highly dynamic scenarios (e.g., egocentric wrist-camera views), where rapid viewpoint shifts and object motion can violate the short-term temporal continuity assumption and blur sharp changes in action-to-vision attention. A promising direction for future work is to replace the fixed temporal smoothing with an adaptive prediction module that adjusts its effective window based on motion cues or feature changes (e.g., magnitude of visual dynamics or action-conditioned attention variance), or to learn a lightweight temporal attention network that directly predicts per-token importance from recent history. Such adaptive mechanisms may further improve pruning quality in dynamic environments while retaining the efficiency advantages of VLA-Pruner.